Enriched finite elements for time-harmonic Webster's equation

Rémi Cornaggia, Eric Darrigrand, Loïc Le Marrec, Fabrice Mahé

Enriched finite elements for time-harmonic Webster's equation

R. Cornaggia[a,*], E. Darrigrand[a], L. Le Marrec[a], F. Mahé[a]

[a] *Université de Rennes, CNRS, IRMAR - UMR 6625, F-35000 Rennes, France*

Abstract

This work presents an enriched finite element method (FEM) dedicated to the numerical resolution of Webster's equation in the time-harmonic regime, which models many physical configurations, *e.g.* wave propagation in acoustic waveguides or vibration of bars with varying cross-section. Building on the wave-based methods existing in the literature, we present new enriched finite element bases that account for both the frequency of the problem and the heterogeneity of the coefficients of the equation. The enriched method is compared to the classical fifth-order polynomial FEM, and we show they share the same asymptotic convergence order, present the same easiness of implementation and have similar computational costs. The main improvement brought by these enriched bases relies on the convergence threshold (the mesh size at which the convergence regime begins) and the convergence multiplicative constant, which are observed to be (i) better than the ones associated with polynomial bases and (ii) not only dependent on the resolution (the number of elements per wavelength), but also on the frequency for a fixed resolution, making the method we propose well adapted to high-frequency regimes. Moreover, taking into account the heterogeneity of the coefficient in Webster's equation by using an element-dependent enrichment leads to a significant decrease of the approximation error on the considered examples compared to a uniform enrichment, again with almost no additional cost. Several possible extensions of this work are finally discussed.

Keywords: Wave-based finite element method, Webster's equation, bar vibrations, high frequency

1. Introduction

This work proposes a finite element method (FEM) adapted to the resolution of problems modeled by the 1D time-harmonic Webster's equation (also called Webster's horn equation):

$$-(\mathcal{A}u')' - k^2\mathcal{A}u = f \tag{1}$$

where the variable coefficient $\mathcal{A} > 0$ will be called the *profile* in the sequel, and the coordinate x belongs to a domain Ω. Webster's equation has been used for a long time to model the vibrations of bars or the propagation of acoustic waves in tubes filled with perfect fluids [8]. Moreover, it may be a relevant approximation of two- or three-dimensional physical models, *e.g.* to describe the acoustic field in axisymmetric waveguides [15], or the acoustic perturbation around a mean flow in ducts [26]. In this work, we will focus for simplicity on the vibrations of bars and on bounded domains Ω.

The FEM [9, 17] and other related methods have also been studied for a long time and their efficiency is well-established to address many physics-inspired problems. However, some problems, including the simulation of wave propagation at high frequency, are still quite difficult to handle. Indeed, the traditional low-degree polynomial elements require a thin mesh, and therefore a prohibitive computational cost, to catch fast oscillations.

To tackle this difficulty, a first possibility is to increase the degree of the considered polynomial bases, as developed by [18, 25] and the references therein. A popular alternative is to rely on *wave-based* (or

*Corresponding author
Email address: remi.cornaggia@univ-rennes1.fr

knowledge-based) methods, which became popular in the 90s, see [19, 17] and the references therein for the first steps in this direction. The main idea is to use exact or approximate solutions of the equation of interest, *e.g.* plane waves for the Helmholtz equation in 2D or 3D, instead of polynomials, to build or enrich approximation spaces. Many of these methods belong to the class of Trefftz methods [16], *e.g.* the *Ultra Weak Variational Formulation* (UWVF) [20], the *wave-based discontinuous Galerkin (DG) method* [23] or the *Discontinuous Enrichment Method* (DEM) [28]. These methods use local bases made entirely of exact or approximated solutions of Helmholtz equation. Another approach is to begin with a classical basis and to add functions of interest in the approximation space, which is the purpose of the *Partition of Unity Method* (PUM) of [24], and its descendant the *Generalized FEM (GFEM)* [27], whose ideas are still found in recent works [11].

These methods were first applied to Helmholtz equation with constant coefficients, see again [19] or the more recent works [10, 16] for reviews. In particular, GFEM-inspired enrichment was proposed in 1D by [3] to find eigenfrequencies of bars and trusses, and also by [21, 14] to solve time-harmonic and then transient wave-related problems. Helmholtz equation with variable coefficients is at our knowledge a bit less studied, but in 1988 [4] proposed already an enrichment strategy dedicated to this equation in 1D and at high wavenumbers, and many recent works *e.g.* [20, 28, 11, 13] provide theoretical and numerical insights on this equation (mostly in 2D, although a part of [20] is dedicated to 1D problems). We refer to the comprehensive reviews provided [11, 13] for more references.

In this context, we propose a PU-inspired enrichment method dedicated to Webster's equation, that presents the following features:

- The classical FEM framework is retained, *i.e.* we use (i) the usual variational formulations of the considered problems and (ii) a Galerkin space of continuous functions $\mathcal{V}_h \subset H^1(\Omega)$, as opposed to alternative formulations or spaces of discontinuous functions used by *e.g.* the UWVF [20], DG [23], DEM [28] and others.

- We enrich the classical space of piecewise linear functions $\mathcal{P}_1$ by adding four inner functions to each elementary basis $\mathbb{P}_1$. By "inner" we mean that each of these functions is supported by one element and vanishes at the mesh nodes, so that the nodal values are still associated with the $\mathbb{P}_1$ "hat" functions only. These functions are built following the PUM and choosing (i) "half-hat" functions (restrictions of "hat" functions to one element) as partition of unity and (ii) two oscillating functions as the enrichment family. This choice of "half-hat" PU is at our knowledge a novelty of this work.

- We first consider the classical enrichment family $\{\sin(kx), \cos(kx)\}$, *i.e.* the basis of solutions to (1) for constant profiles and $f = 0$, as in *e.g.* [3]. The associated enriched basis is noted $\mathbb{P}^k_{1,4}$. We then introduce a more general family of bases denoted by $\mathbb{P}^{k,\delta}_{1,4}$, that depend on a parameter $\delta \in \mathbb{R}$ (so that $\mathbb{P}^{k,0}_{1,4} = \mathbb{P}^k_{1,4}$), and that account for the local variations of the profile $\mathcal{A}$: the considered oscillating functions are solutions of (1) for *exponential* profiles $\mathcal{A}(x) = \mathcal{A}_0 e^{2\delta x}$ and $f = 0$.

- Using these enriched bases is shown to induce a comparable behavior of the FEM than using a hierarchical basis $\mathbb{P}_5$ of fifth-order polynomials, in the sense that (i) the same asymptotic rate of convergence is reached in terms of the mesh size h and (ii) the same procedures can be used to build the FE matrices, which have the same size and sparsity.

- As a result, the *static condensation* procedure is applicable to the resulting linear systems, as for the DEM [28], and the conditioning of the condensed systems obtained using enriched and polynomials bases are almost equal. This tackles a usual drawback of wave-enriched methods, which often lead to ill-conditioned systems without proper treatment [27, 16, 23].

- For the case $f = 0$, we observe on numerical examples that the asymptotic convergence regime begins earlier for enriched solutions than for polynomial ones. Moreover, for a given resolution (the number of points per wavelength), the enriched solution converges at high frequencies, *i.e.* the error decreases as k increases.

- A profile-dependent enrichment procedure, where a parameter δ_n is computed and the basis $\mathbb{P}^{k,\delta_n}_{1,4}$ is used for the n-th element, is finally presented and compared with the uniform enrichment that uses the same basis $\mathbb{P}^{k}_{1,4}$ for all elements. The FEM error is reduced by a factor up to 2 in the considered numerical examples, at a very slight additional computational cost.

This paper is organized as follows. We begin in Section 2 by presenting the boundary value problems we focus on and the corresponding weak formulations, and by recalling some classical results and notations about the FEM used throughout the paper. Section 3 specifies how we build an enriched basis by using the "half-hat" partition of unity and sines and cosines as enrichment functions. The computational and interpolation properties of this basis are studied and compared with a fifth-order polynomial basis, and numerical examples are provided. This method is then generalized in Section 4, where we define a family of element-dependent enrichment functions that account for the variability of the profile $\mathcal{A}$. Numerical results again highlight the advantages of this generalization. Finally, we discuss our results and present possible extensions in Section 5, and we summarize and highlight the key points of our work in Section 6. Some auxiliary results and proofs are gathered in appendices.

2. Problem definition

As mentioned in the introduction, the field u of interest obeys Webster's equation:

$$-\left(\mathcal{A}u'\right)' - k^2\mathcal{A}u = f, \quad \text{in } \Omega. \tag{2}$$

To fix ideas, we assume hereinafter that this equation models the vibrations of a geometrically heterogeneous straight bar in a dimensionless setting, as shown in Appendix A. In this case, (i) the domain of interest is $\Omega =]0, L[$ where L is the non-dimensional length of the bar, (ii) the profile $\mathcal{A}$ corresponds to the area of the cross-section, (iii) the field u is the amplitude of the longitudinal displacement of the cross-sections and $\sigma := \mathcal{A}u'$ is the traction they support and (iv) f is the amplitude of a time-harmonic density of forces. Eq. (2) must be completed by boundary conditions. In this work, we consider only displacement and traction (*i.e.* Dirichlet and Neumann) boundary conditions, and we focus on cantilever (ct) and clamped–clamped (cc) bars corresponding to:

$$\text{(ct)} \ : \quad \{u(0) = 0,\ \sigma(L) = \left(\mathcal{A}u'\right)(L) = \sigma_\star\}, \qquad \text{(cc)} \ : \quad \{u(0) = 0,\ u(L) = u_\star\}. \tag{3}$$

We also define the dimensionless characteristic wavelength λ as:

$$\lambda = 2\pi/k. \tag{4}$$

2.1. Variational formulations and well-posedness of the problems

The variational (or weak) formulations of the problems above are obtained by multiplying the equation (2) by a test function v, integrating over the domain Ω and integrating by parts. We then look for a solution u belonging to a *trial space* $\mathcal{V}$ (or space of kinematically admissible displacements) that satisfies the resulting equality for any test function v belonging to a *test space* $\mathcal{V}_0$, *i.e.* :

$$\text{Find } u \in \mathcal{V}, \quad \int_0^L \mathcal{A}(u'v' - k^2uv) = \Big[\mathcal{A}u'v\Big]_0^L + \int_0^L fv, \quad \forall v \in \mathcal{V}_0. \tag{5}$$

This is the classic weak formulation for the studied boundary-value problems, where the trial and test functional spaces $(\mathcal{V}, \mathcal{V}_0)$ are subspaces of H^1 (where H^1, with the domain unspecified, means $H^1(\Omega)$ hereinafter, as well as other Sobolev spaces *e.g.* L^2) and depend on the choice of boundary conditions, along with the value taken by the right-hand side.

For instance, for cantilever bars we have $\mathcal{V} = \mathcal{V}_0 = H^1_{(0} := \{u \in H^1,\ u(0) = 0\}$ and the weak form of the problem is:

$$\text{(ct)} \quad \text{Find } u \in H^1_{(0}, \quad \int_0^L \mathcal{A}(u'v' - k^2uv) = \sigma_\star v(L) + \int_0^L fv, \quad \forall v \in H^1_{(0}. \tag{6}$$

For clamped–clamped bars, the trial space is $\mathcal{V} = H^1_\star := \{u \in H^1,\ u(0) = 0,\ u(L) = u_\star\}$, while the test space is $\mathcal{V}_0 = H^1_0 = \{u \in H^1,\ u(0) = 0,\ u(L) = 0\}$, and (5) becomes,

$$\text{(cc)} \quad \text{Find } u \in H^1_\star, \quad \int_0^L \mathcal{A}(u'v' - k^2uv) = \int_0^L fv, \quad \forall v \in H^1_0. \tag{7}$$

In this case, and more generally when a non-homogeneous displacement boundary condition is required, the trial space differs from the test space. To come back to the comfortable situation where $\mathcal{V} = \mathcal{V}_0$, we use the lifting $u = \hat{u}_\star + w$, where $\hat{u}_\star$ may be any function of $H^1_\star$. Then the new unknown w is the solution of the equivalent problem (denoted (lcc) for lifted-(cc)):

$$\text{(lcc)} \quad \text{Find } w \in H^1_0, \quad \int_0^L \mathcal{A}(w'v' - k^2wv) = \int_0^L fv - \int_0^L \mathcal{A}(\hat{u}'_\star v' - k^2\hat{u}_\star v), \quad \forall v \in H^1_0. \tag{8}$$

Concerning the well-posedness of these problems, we first underline our choice to enforce only displacement and traction boundary conditions, as opposed to Robin boundary conditions such as $(u' - \mathrm{i}ku)(L) = g_\star$. Indeed, the later conditions are very often used – see *e.g.* [4, 19, 10] – because (i) they mimic absorbing boundary conditions used for scattering problems in higher dimensions and (ii) the resulting (complex-valued) sesquilinear form is elliptic, which guarantees the well-posedness of the problem. In our case, to tackle the loss of ellipticity, we have to make the important additional assumption that k^2 is not an eigenvalue of any of the considered problems. Under this assumption, (ct) and (lcc) are well-posed, as shown *e.g.* in [17] using Fredholm alternative, in [5] using the modern approach of T-coercivity or in [13]. Note that this assumption does not ensure that the discrete problems defined thereafter are well-posed for each discretization, as eigenvalues of the discrete problems may differ from those of the continuous problems.

Remark 1. *Since, up to a lifting, we can always come back to the case $\mathcal{V} = \mathcal{V}_0$ for any variational problem, we will present only clamped–clamped rods in the upcoming numerical examples. However, the (ct) case was implemented and we observed the same convergence properties in both cases, except near eigenvalues, which are not the same for the two problems.*

2.2. Finite element method

As mentioned in the introduction, to solve variational problems of the form (5) with rough profiles $\mathcal{A}$ or nonzero force density f, we chose to focus on the finite element method (FEM). It belongs to the class of Galerkin methods, *i.e.* it relies on an approximation of the trial space $\mathcal{V}$ by a finite-dimension subspace $\mathcal{V}_h \subset \mathcal{V}$ of dimension N_h.

By defining a basis $\{\phi_n\}_{n=0\dots N_h}$ of $\mathcal{V}_h$, looking for an approximation $u_h = \sum_n u_n\phi_n$ of u, and using the ϕ_n as test functions, writing the discretized variational formulation results in the linear system:

$$(\boldsymbol{K} - k^2\boldsymbol{M}) \cdot \boldsymbol{u} = \boldsymbol{f}, \tag{9}$$

where $\boldsymbol{u} = (u_n)_{n=0\dots N_h}$ is the vector of unknowns, $\boldsymbol{K}$ and $\boldsymbol{M}$ are the stiffness and mass matrices associated with the basis $\{\phi_n\}_{n=0\dots N_h}$ and the profile $\mathcal{A}$, whose components are:

$$K_{ij} = \int_0^L \mathcal{A}\phi'_i\phi'_j \quad \text{and} \quad M_{ij} = \int_0^L \mathcal{A}\phi_i\phi_j, \tag{10}$$

and $\boldsymbol{f}$ is the vector of source terms: it accounts for the force density f, the traction boundary condition in the (ct) case and the contribution of $\hat{u}_\star$ in the (lcc) case. Ultimately, solving the linear system (9) gives an approximation $u_h \in \mathcal{V}_h$ of u. For more details on the FEM and some references, notably on the choices of spaces $\mathcal{V}_h$ and practical implementation procedures, we refer to textbooks *e.g.* [17, 9].

Remark 2. *It is often more convenient to define $\mathcal{V}_h$ as a subspace of H^1 (instead of $\mathcal{V}$), and then look for an approximated solution u_h in $\mathcal{V}_h \cap \mathcal{V}$,* i.e. *consider $\mathcal{V}_h$ together with the boundary conditions defining $\mathcal{V}$. This is the viewpoint we will adopt thereafter.*

The efficiency of the FEM depends on the choice of the approximation space $\mathcal{V}_h$ through the well-known stability result that links the approximation error $\|u-u_h\|_{H^1}$ to the interpolation properties of $\mathcal{V}_h$:

Lemma 1. *[6, Thm. 1 and 2] There exist a threshold $h_0>0$ and a constant $C>0$ such that:*

$$\forall\ h<h_0, \qquad \|u-u_h\|_{H^1} \leq C \inf_{w_h\in\mathcal{V}_h} \|u-w_h\|_{H^1}. \tag{11}$$

For the static case ($k=0$), this is *Céa's lemma*, which holds for any h (*i.e.* $h_0=+\infty$), thanks to the ellipticity of the bilinear form in (5).

For $k\neq 0$, we refer to the proofs given in [6] in a general context, or again to the more specific approaches for Helmholtz-like problems provided by [5, Thm. 2 and Sect. 3] and by [13, Thm 4.1]. In this case the threshold $h_0<+\infty$ depends on the wavenumber k: it typically decreases as k increases, *e.g.* [4, Thm 3.1] finds $h_0=c^\star k^{-2}$ for some $c^\star>0$ for a related problem. This threshold will be of particular importance when discussing the relevance of the enriched spaces that we present in the next sections.

Remark 3. *In* (11)*, we omitted for simplicity the additional terms coming from the approximation of integrals such as* (10) *by quadrature formulas, as specified by [5, Thm. 2]. However, in all the numerical experiments that we present, we made sure that their contribution is negligible with respect to the approximation error by taking a large enough number of quadrature points.*

3. Enriched FEM using "half-hat" partition of unity

In this section, we build a first $\mathbb{P}_1$-enriched finite element basis noted $\mathbb{P}^k_{1,4}$, where the "half-hat" partition of unity is used while sines and cosines are chosen as enrichment functions, taking advantage of the prior knowledge of the fixed wavenumber k. A comparison with a fifth-order polynomial basis $\mathbb{P}_5$ is conducted, with a proof that the two associated spaces $\mathcal{P}^k_{1,4}$ and $\mathcal{P}_5$ share the same interpolation convergence properties, and numerical illustrations of the improvements brought by the proposed method.

3.1. Partition of unity method and sine-enriched basis

We adopt the viewpoint of the partition of unity (PU) method as defined in [24], which can be summarized as follows. One must first define a PU $\{\varphi_n\}_{n=0\dots N}$, *i.e.* a family of functions such that:

$$\sum_{n=0}^{N}\varphi_n(x)=1, \quad \forall x\in\Omega.$$

Given another "enrichment" family $\Psi=\{\psi_m\}_{m=1\dots N_m}$, which gathers functions that we would like to add in the approximation space, one then builds an *enriched function space* $\mathcal{V}_h^\Psi$ as:

$$\mathcal{V}_h^\Psi=\operatorname{span}\{\varphi_n^m\}_{n=0\dots N,\ m=0\dots N_m} \quad \text{with} \begin{cases} \varphi_n^0=\varphi_n, \\ \varphi_n^m=\varphi_n\psi_m \quad \text{for } m=1\dots N_m. \end{cases} \tag{12}$$

A function $u_h\in\mathcal{V}_h^\Psi$ is defined by the $(N+1)\times(N_m+1)$ values u_n^m so that:

$$u_h=\sum_{n=0}^{N}\sum_{m=0}^{N_m} u_n^m\varphi_n^m. \tag{13}$$

The most commonly used PU is the family of "hat" functions, to which the notation φ_n will apply hereafter, defined from a mesh $\Omega_h=\{x_0\dots x_N\}$ of $[0,L]$ as plotted in Figure 1. Indeed, these functions are a basis of the traditional piecewise-linear FE space $\mathcal{P}_1$, see [9, Sec. 1.1.2], and this choice permits to retain some convenient properties of this basis for the enriched space, notably the sparsity of stiffness and mass matrices, see again [24, 27]. In [3, 21, 14] among others, this PU is combined with enrichment families containing oscillating functions with various wavenumbers.

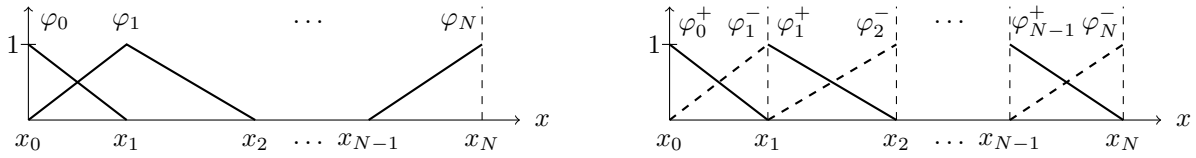

Figure 1: "Hat" (left) and "Half-hat" (right) functions defined from a mesh $\{x_0, ..., x_N\}$.

Our approach differs on several points. First, we use the PU of "half-hat" functions $\{\varphi_n^-\}_{n=1...N}$ and $\{\varphi_n^+\}_{n=0...N-1}$, whose supports are the elements $I_n = [x_{n-1}, x_n]$ for the φ_n^- and $I_{n+1} = [x_n, x_{n+1}]$ for the φ_n^+, as represented in Figure 1. More precisely, noting $h_n = x_n - x_{n-1}$ the length of an element I_n, they are:

$$\varphi_n^-(x) = \begin{cases} \dfrac{x - x_{n-1}}{h_n} & \text{if } x \in I_n \\ 0 & \text{elsewhere} \end{cases} \qquad \varphi_n^+(x) = \begin{cases} \dfrac{x_{n+1} - x}{h_{n+1}} & \text{if } x \in I_{n+1} \\ 0 & \text{elsewhere} \end{cases}. \tag{14}$$

Second, we use only the wavenumber k associated with the considered time-harmonic excitations, and use sines and cosines as enrichment family:

$$\Psi^k = \{\sin(kx), \cos(kx)\}. \tag{15}$$

From a more physical point of view, this enrichment introduces in the FE basis the solutions associated with a bar with *constant cross-section* submitted to time-harmonic boundary excitations only, *i.e.* the solutions of (2) for constant $\mathcal{A}$ and $f = 0$.

Third, we want the additional basis functions to vanish at all nodes x_n, which will enable (i) to easily apply boundary conditions and (ii) to use the static condensation procedure. Following (12), we attribute *a priori* six functions to each interior node, defined by:

$$\begin{aligned} &\varphi_n^{0\pm}(x) = \varphi_n^{\pm}(x), \\ &\varphi_n^{1\pm}(\xi) = \varphi_n^{\pm}(x) \sin\left(k(x - x_n)\right), \\ &\varphi_n^{2\pm}(\xi) = \varphi_n^{\pm}(x) \left(\cos\left(k(x - x_n)\right) - 1\right), \end{aligned} \tag{16}$$

and three functions to each of the end points: $\{\varphi_0^{m+}\}_{m=0...2}$ to x_0 and $\{\varphi_N^{m-}\}_{m=0...2}$ to x_N. Note that the functions defined by (16) are all continuous on Ω except the $\varphi_n^{0\pm}$. The continuity of a linear combination u_h of these functions must therefore be imposed for the enriched space to be a subspace of H^1. It is done by attributing the same coefficient to φ_n^{0-} and φ_n^{0+} for $n = 1 \dots N-1$ in such linear combinations, *i.e.* we consider functions u_h of the form:

$$u_h = \sum_{n=0}^{N} u_n^0 \varphi_n^0 + \sum_{n=1}^{N-1} \sum_{m=1}^{2} \left[u_{n-1}^{m+} \varphi_{n-1}^{m+} + u_n^{m-} \varphi_n^{m-} \right], \tag{17}$$

where we use the notations $\varphi_0^0 = \varphi_0^{0+}$, $\varphi_n^0 = \varphi_n^{0-} + \varphi_n^{0+} = \varphi_n$ for $n = 1 \dots N-1$ and $\varphi_N^0 = \varphi_N^{0-}$. In the sum (17), the distinction is made between the *nodal values* u_n^0 associated with the $\mathbb{P}_1$ basis functions, and the *inner values* $u_n^{m\pm}$ associated with the additional functions whose supports are the elements I_n only, thanks to the choice of the "half-hat" PU. The approximation space we have built is:

$$\mathcal{P}_{1,4}^k = \text{span}\left\{ \{\varphi_n^0\}_{n=0...N} \bigcup \{\varphi_{n-1}^{m+}, \varphi_n^{m-}\}_{n=1...N,\ m=1,2} \right\}, \quad \dim \mathcal{P}_{1,4}^k = 5N + 1. \tag{18}$$

Finally, specifying the Dirichlet boundary conditions corresponding to a given problem, *i.e.* defining subspaces of $H^1_{(0}$ or H^1_0, is done by fixing the boundary values $u_0^0 = u_h(0)$ and $u_N^0 = u_h(L)$. The dimensions of the approximation spaces $\mathcal{P}_{1,4}^k \cap H^1_{(0}$ and $\mathcal{P}_{1,4}^k \cap H^1_0$ are therefore $5N$ and $5N - 1$.

Remark 4. *As a consequence of our choice of boundary conditions for (ct) and (lcc), u is real-valued (for real-valued f) and therefore we chose to stick to real-valued functions to define the enrichment space Ψ^k in* (15)*, as also done* e.g. *in [14]. The equivalent family $\{\exp(\pm \mathrm{i}kx)\}$ could be used instead as in [21]* e.g. *when absorbing-like Robin boundary conditions are applied.*

To conclude the presentation of the sine-enriched space $\mathcal{P}^k_{1,4}$, the following theorem gives interpolation properties which permit to bound the approximation error as specified by Lemma 1.

Theorem 2. *Consider the space $\mathcal{P}^k_{1,4}$ defined by* (18) *from a mesh $\{x_0 \dots x_N\}$. Let $I_n = [x_{n-1}, x_n]$ denote the n-th element, and h_n denote its length, and define the maximal element length $h := \max_{n=1\dots N} h_n$. Then for any function $u \in C^0(\Omega) \cap \left\{u \mid u_{|I_n} \in C^6(I_n),\ \forall n = 1 \dots N\right\}$, there exists a constant C_u that depends on u and k but not on h such that, for h small enough,*

$$\inf_{w_h \in \mathcal{P}^k_{1,4}} \left(\sum_{n=1}^{N} \|u - w_h\|^2_{L^2(I_n)} \right)^{1/2} \leq C_u h^6 \quad \textit{and} \quad \inf_{w_h \in \mathcal{P}^k_{1,4}} \left(\sum_{n=1}^{N} \|u' - w_h'\|^2_{L^2(I_n)} \right)^{1/2} \leq C_u h^5. \tag{19}$$

To ease the presentation, the proof of this theorem is given in Appendix C. Note that the hypothesis we used on the regularity of u (piecewise C^6 instead of H^6) is not completely conventional. This choice comes from (i) a technical necessity specified by Remark 7 at the end of the proof and (ii) the following physical considerations: the functions u of interest in this study are the weak solutions of $-(\mathcal{A}u')' - \mathcal{A}k^2 u = f$ with possibly irregular profile $\mathcal{A}$ and/or force density f. Such solutions are continuous, but may not be more regular on the whole interval Ω. However, for practical applications, $\mathcal{A}$ is piecewise C^∞ and f can be decomposed into the sum $f = f_\mathrm{c} + f_\mathrm{p}$, where f_c is a piecewise C^∞ density of forces and f_p is a sum of Dirac distributions that represents punctual forces. By choosing a mesh whose nodes match with (i) the discontinuities of $\mathcal{A}$ and f_c and all their derivatives and (ii) the points supporting punctual forces, we ensure that u is also C^∞ inside each of the elements of the mesh and therefore satisfies the theorem.

3.2. Comparison with fifth-order polynomial basis and implementation considerations

The performance of the proposed method is compared with the well-documented approximation space $\mathcal{P}_5$ of continuous and piecewise-polynomial functions, with degree up to 5. Indeed, this space shares the same asymptotic interpolation behavior as $h \to 0$ with the enriched space $\mathcal{P}^k_{1,4}$. Moreover, the elementary bases of these spaces both include two "nodal" functions and four "inner functions", which enables to (i) use the same procedures for the matrices computations and (ii) apply the static condensation algorithm to the linear system (9), as explained now.

Interpolation properties. A convergence result close to the one given by Theorem 2 holds:

Proposition 1. *Consider the space $\mathcal{P}_5$ of continuous and piecewise fifth-order polynomial functions, associated with a mesh $\{x_0 \dots x_N\}$. Then for any function $u \in C^0(\Omega) \cap \left\{u \mid u_{|I_n} \in H^6(I_n),\ \forall n = 1 \dots N\right\}$, there exists a constant $C > 0$ such that, for any h,*

$$\begin{aligned} &\inf_{w_h \in \mathcal{P}_5} \left(\sum_{n=1}^{N} \|u - w_h\|^2_{L^2(I_n)} \right)^{1/2} \leq C \left(\sum_{n=1}^{N} \|u^{(6)}\|^2_{L^2(I_n)} \right)^{1/2} h^6, \\ \textit{and} \quad &\inf_{w_h \in \mathcal{P}_5} \left(\sum_{n=1}^{N} \|u' - w_h'\|^2_{L^2(I_n)} \right)^{1/2} \leq C \left(\sum_{n=1}^{N} \|u^{(6)}\|^2_{L^2(I_n)} \right)^{1/2} h^5. \end{aligned} \tag{20}$$

This is a classical result for $\mathcal{P}_5$, see *e.g.* [17, Lemma 4.17] or [9, Prop. 1.12] for proofs. Note that by contrast with Theorem 2, (i) u is only required to be in H^6 (and not C^6) in each element, (ii) the results hold for any h and (iii) the dependency of the multiplicative constant noted C_u in Theorem 2 is explicit in u.

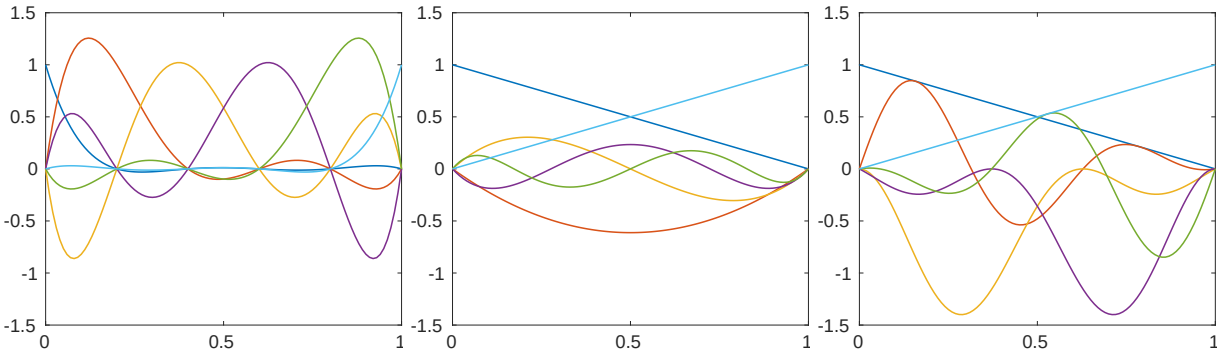

Figure 2: Basis functions on an element of length $h = 1$. From left to right, nodal basis of Lagrange polynomials (here with regularly spaced inner nodes), hierarchical basis of Lobatto polynomials, and sine-enriched basis $\mathbb{P}^k_{1,4}$ for $k = 10$.

Elementary bases. Several choices are possible for an elementary basis of $\mathcal{P}_5$. One is the nodal basis based on Lagrange interpolation polynomials presented in [9, Sec. 1.1.3], where all the shape functions are fifth-order polynomials. Another is the hierarchical basis of Lobatto polynomials of increasing order given by [17, Sec. 4.7] and recalled in Appendix B.

These two bases, along with our sine-enriched basis, are plotted in Figure 3.2. They all feature six functions per element, two of them associated with the nodal values (which are degrees of freedom shared with adjacent elements), and the four other being "inner" functions vanishing at both extremities. Consequently, the finite element computation process is identical for the three bases: the matrices are assembled by the same routine, the boundary conditions are enforced in the same way and the final linear systems to be solved have the same size and sparsity. In other words, adding our basis in an existing code which handles the classical polynomial spaces requires almost no work: one only has to add the functions defined by (16) in the FE library, and then call the existing procedures associated with $\mathcal{P}_5$.

Comparing the two available bases for polynomial spaces $\mathcal{P}_p$, [9, Sec. 1.1.5] shows that hierarchical bases have some advantages over Lagrange nodal bases, notably the good conditioning of the stiffness matrix (whose blocks corresponding to internal values are diagonal for Lobatto polynomials and constant $\mathcal{A}$) and the ease for increasing the polynomial order p. In this work, we consider non-constant profiles and we focus on $p = 5$, but easily increasing the polynomial order is a feature we would like to retain for a perspective we will discuss in Section 5. We therefore use the Lobatto basis and denote it by $\mathbb{P}_5$ hereinafter.

Numerical integration. To compute the integrals (10), we used a classical Gauss quadrature [9, Sect. 8] and the following procedure to ensure that the integration of oscillatory basis functions remains accurate even for large elements supporting several wavelengths. First each element is divided into $N_{\text{se}} := \lceil h/\lambda \rceil$ subelements of equal lengths, where $h = \max_{n=1\ldots N} h_n$ and $\lceil \cdot \rceil$ denotes the ceiling function so that $\lceil x \rceil - 1 < x \leq \lceil x \rceil$ for any $x \in \mathbb{R}$. In this way, each subelement is smaller than the characteristic wavelength λ. Then, 10 Legendre–Gauss points are used in each subelement to compute its contribution to the total integral. In particular, when $h < \lambda$ one has $\lceil h/\lambda \rceil = 1$ and 10 points per element are used. In the asymptotic convergence regime, the quadrature error therefore behaves as $O(h^{20})$ and is negligible with respect to the interpolation error, as announced in Remark 3.

Static condensation. Finally, and perhaps most importantly, *static condensation* (SC) can be applied to the linear system (9) when both bases $\mathbb{P}_5$ and $\mathbb{P}^k_{1,4}$ are used. This procedure is described in detail in [17, Sec. 4.7.3]. In short, it intervenes (i) in the matrices assembly process so that only the nodal values are retained as degrees of freedom for the linear system to be solved, and (ii) as a post-processing operation (the decondensation) to retrieve the inner values from the node values. In particular, after step (i) the matrix to be inverted has the same size than the one that would be obtained with piecewise-linear elements $\mathbb{P}_1$ (*e.g.* $N \times N$ instead of $5N \times 5N$ for the (ct) case), the same sparsity (the nonzero values are all on the upper, middle and lower diagonals), and the system is better conditioned than the original one. This possibility

is a major advantage of the proposed enriched spaces, as wave-based methods are often badly conditioned and not always suitable for static condensation (see *e.g.* [27] for the generalized finite element method, [16] for Trefftz methods and [23] for a wave-based discontinuous Galerkin method), another exception being the discontinuous enrichment method [28] for which static condensation is also applicable.

3.3. Numerical illustrations

In the numerical illustrations, we use the *resolution* $\lambda/h = 2\pi/kh$, *i.e.* the number of elements per wavelength, as the indicator of the numerical cost, rather than the number of elements which is less relevant to compare solutions obtained for different wavenumbers. In particular, we focus on the range $0.1 < \lambda/h < 10$, to show how the sine-enriched basis can overcome the "rule of thumb" which imposes several elements per wavelength for polynomial bases *i.e.* $\lambda/h > 1$.

To this end, we implemented the finite element bases described above in a home-made MATLAB code, performed computations at several resolutions for some problems described hereafter, and compared them using a discrete version of the relative H^1 error. This error is computed as follows:

$$E(u_h) = \left(\sum_{n=0}^{N_E} |u(y_n) - u_h(y_n)|^2 + |u'(y_n) - u_h'(y_n)|^2 \right)^{1/2} \Bigg/ \left(\sum_{n=0}^{N_E} |u(y_n)|^2 + |u'(y_n)|^2 \right)^{1/2}, \qquad (21)$$

where u_h is an approximation of u, and the same dedicated regular mesh $\{y_n\}_{n=0\dots N_E}$ with $N_E = 4000$ is used in all the examples hereinafter, so that there are always at least 10 points per wavelength for the error computation.

We note $u_h^{(5)}$ (resp. u_e^k) an approximation obtained using the space $\mathcal{P}_5$ (resp. $\mathcal{P}_{1,4}^k$). Combining the stability result of Lemma 1 and the interpolation properties given by Theorem 2, the discrete error (21) is supposed to behave like $O(h^5)$ for these two approximations, and the main differences are expected to lie on the value of the threshold h_0 at which the asymptotic convergence sets in, and on the multiplicative constants.

In this part, we consider a bar of length $L = 10$ with quadratic profile $\mathcal{A}(x) = (1 + \alpha x)^2$ (with $\alpha = 0.2$ for the forthcoming computations). Such a bar is represented in Figure 3. We consider the configuration (cc) with $u_\star = 1$, and look at the FE solutions without and with force densities.

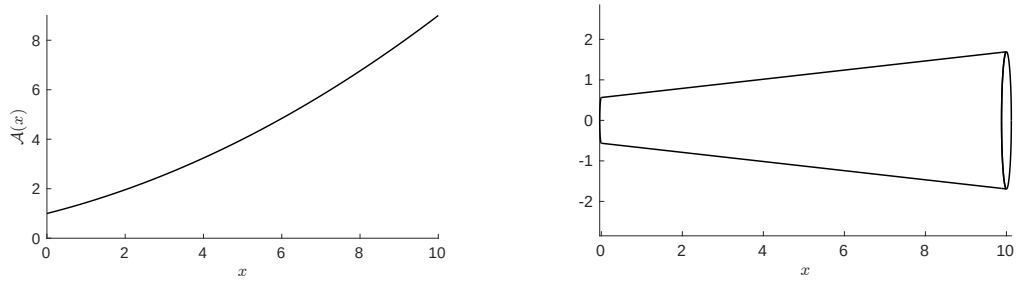

Figure 3: Quadratic profile (left) and corresponding bar with circular cross-section and radius $r(x) = \sqrt{\mathcal{A}(x)/\pi} = (1 + \alpha x)/\sqrt{\pi}$ (right).

Boundary excitations only. We begin by setting $f = 0$. In this case, the analytic solution, as given in Appendix A, is:

$$u(x) = \frac{1 + \alpha L}{\sin(kL)} \frac{\sin(kx)}{1 + \alpha x}. \qquad (22)$$

A first qualitative illustration is given by Figure 4 in which the FE solutions are compared for a medium resolution $\lambda/h \approx 1$. For the displacement (left panel), the sine-enriched solution is superposed with the exact solution, while the polynomial solution has a slight misfit. This misfit is more clear when looking at the traction $\sigma = \mathcal{A}u'$ (right panel), for which the polynomial solution exhibits spurious discontinuities while the

sine-enriched solution still matches perfectly with the exact one. The associated errors are $E(u_e^k) = 0.44\%$ and $E(u_h^{(5)}) = 8.1\%$.

A more quantitative overview is provided by Figure 5, where the errors are plotted for several wavenumbers, and at similar resolutions (left panel). It is also clearly seen that the threshold h_0 at which the convergence sets in is much higher for the sine-enriched solution than for the polynomial solution. Indeed, the later requires around one element per wavelength to start converging, while the sine-enriched solution converges already for much coarser meshes.

Moreover, for a given resolution the behavior when the wavenumber k increases is not the same. The quality of the polynomial solution depends on the resolution only: the error behaves like $O((kh)^5)$ as showed by [18] for similar problems. On the contrary, the error of the sine-enriched solution decreases for a fixed resolution. We plotted on the right panel of Figure 5 these errors for resolutions fixed to one and two elements per wavelength, and $k \in [1, 100]$. When the convergence regime is established ($\lambda/h = 2$), we observe a convergence rate of approximately $O(k^{-2})$, so that the error $E(u_e^k)$ eventually behaves like $O(k^{-2}(kh)^5)$.

Finally, Figure 6 shows the conditioning numbers of the matrices to be inverted, obtained with the two bases. Without static condensation (*i.e.* when the original system $(\boldsymbol{K} - k^2\boldsymbol{M}) \cdot \boldsymbol{u} = \boldsymbol{f}$ is inverted), using the sine-enriched space leads to a badly-conditioned matrix as the resolution increases, as already observed for other wave-based methods *e.g.* [23], whereas the system obtained with the polynomial space is much less affected. However, applying the static condensation results in an almost equal conditioning for both systems. The computational costs of both methods can therefore be considered to be almost identical.

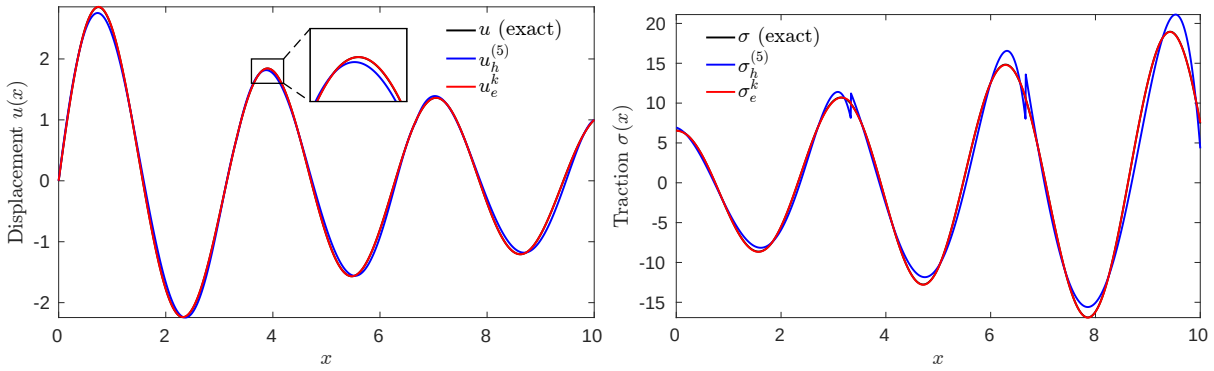

Figure 4: Exact and approximated solutions for the displacement (left) and the traction (right) in a bar with quadratic profile for $k = 2$ and $N = 3$ elements: the resolution is $\lambda/h \approx 0.94$. In both cases, the sine-enriched solution u_e^k (red) is superposed with the exact one (black).

Nonzero forces. The following important step is to look at the behavior of our enriched basis when a nonzero density of forces is applied. In this case, the solution is not only an oscillating function with wavenumber k like the previous one (22), but also presents (possibly rapidly) space-varying components with a characteristic length which is unrelated to λ. To study such a configuration with an analytic solution for the convergence study, we choose a particular solution $u_{\mathrm{P}}(x) = \sin(k_{\mathrm{P}}x)$ and add to the previous problem the corresponding density of forces $f = -(\mathcal{A}u'_{\mathrm{P}})' - \mathcal{A}k^2u_{\mathrm{P}}$. The full solution is therefore $u = u_{\mathrm{P}} + u_{\mathrm{H}}$, where u_{H} satisfies:

$$-(\mathcal{A}u'_{\mathrm{H}})' - k^2u_{\mathrm{H}} = 0, \quad u_{\mathrm{H}}(0) = -u_{\mathrm{P}}(0) = 0, \quad \text{and} \quad u_{\mathrm{H}}(L) = u_\star - u_{\mathrm{P}}(L) = 1 - \sin(k_{\mathrm{P}}L). \tag{23}$$

In this way, if $k_{\mathrm{P}} > k$, the shorter characteristic length in the solution is the one of u_{P}. Again, one can then wonder if the sine-enriched basis, built to handle oscillations at wavenumber k, will succeed to follow faster variations, at least as well as the polynomial basis whose definition is independent of k.

To address this question, we chose the configuration $k_{\mathrm{P}} = \pi k$ (*i.e.* fast variations of the particular solution), for which the solutions are plotted in Figure 7 for $k = 2$ and $N = 7$, so that $\lambda/h \approx 2.2$ and $\lambda_{\mathrm{P}}/h = 2\pi/k_{\mathrm{P}}h = 0.7$. This time the enriched solution performs almost identically than the polynomial

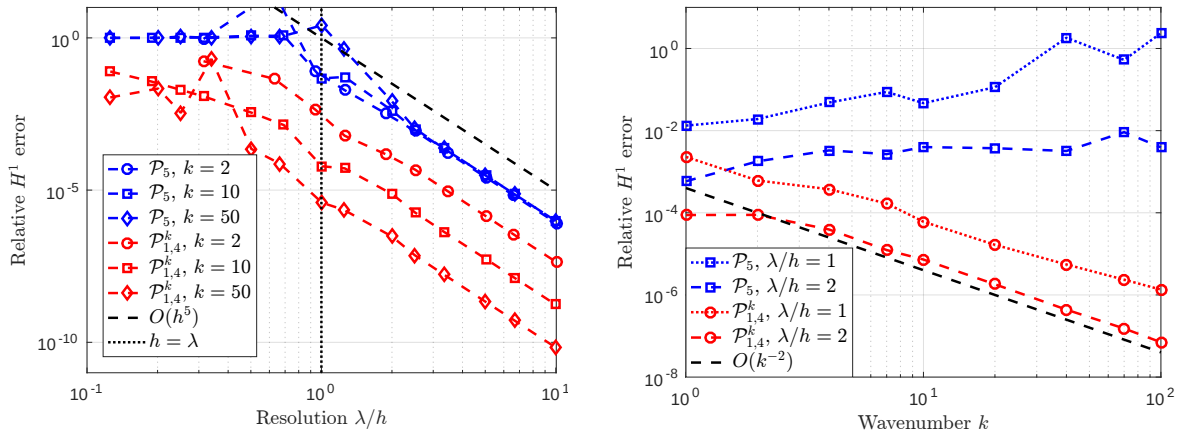

Figure 5: Relative H^1 errors obtained using the polynomial space $\mathcal{P}_5$ (blue) and the enriched space $\mathcal{P}^k_{1,4}$ (red). Left: fixed wavenumbers k and varying resolution λ/h, and right: fixed resolutions and varying wavenumber.

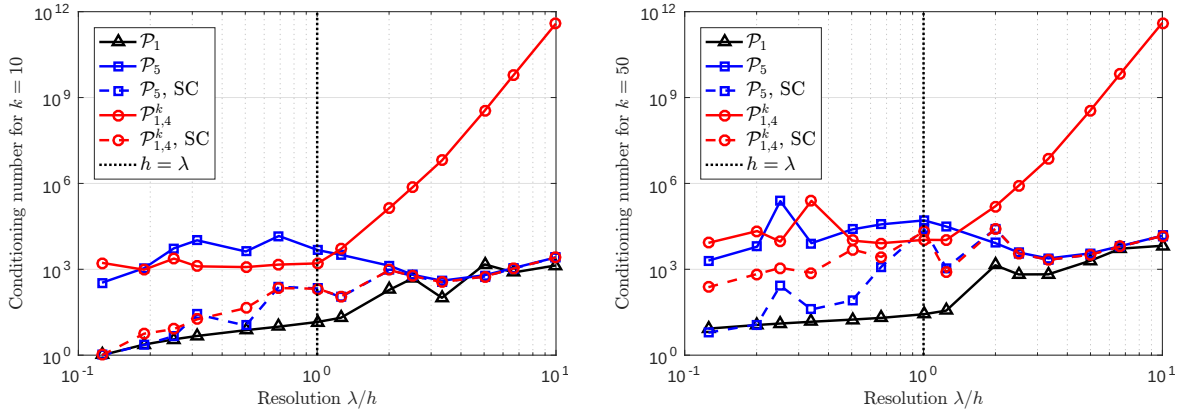

Figure 6: Conditioning number of the system to be solved, obtained without (solid lines) and with (dashed lines) static condensation, for $k=10$ (left) and $k=50$ (right). For comparison purposes, the conditioning of the matrices obtained with the space $\mathcal{P}_1$ of linear-by part elements is also plotted (solid black line).

one: we obtain $E(u^k_e)=20\%$ and $E(u^{(5)}_h)=23\%$. In particular both solutions exhibit discontinuities of the traction. Still for $k_{\mathrm{P}}=\pi k$, this nearly identical behavior is confirmed in Figure 8: the threshold is the same for both bases (and likely determined by k_{P}) for all wavenumbers k, and the enriched basis stays equivalent (and even slightly better for some specific points) than the polynomial basis.

We checked (but did not display the results for brevity) that the sine-enriched basis performs better or equivalently than the polynomial basis for several other values of k_{P} in $[0,\pi k]$. We observed that the improvement decreases when k_{P} becomes close to k and larger (except for $k_{\mathrm{P}}=k$, in which case the particular solution belongs to the approximation space $\mathcal{P}^k_{1,4}$ and is very well captured).

4. Profile-dependent local enrichment via exponential approximation

In this section, we present an enrichment that takes into account not only the wavenumber k, but also the variable profile $\mathcal{A}$. To do so, we enrich each elementary basis with a different family of two oscillating functions, which are solutions of the homogeneous Webster's equation for various *exponential* profiles. The obtained space is therefore locally enriched, by contrast with the uniform enrichment defined in the previous section. Thereafter, we first give some new notations dedicated to exponential profiles and corresponding

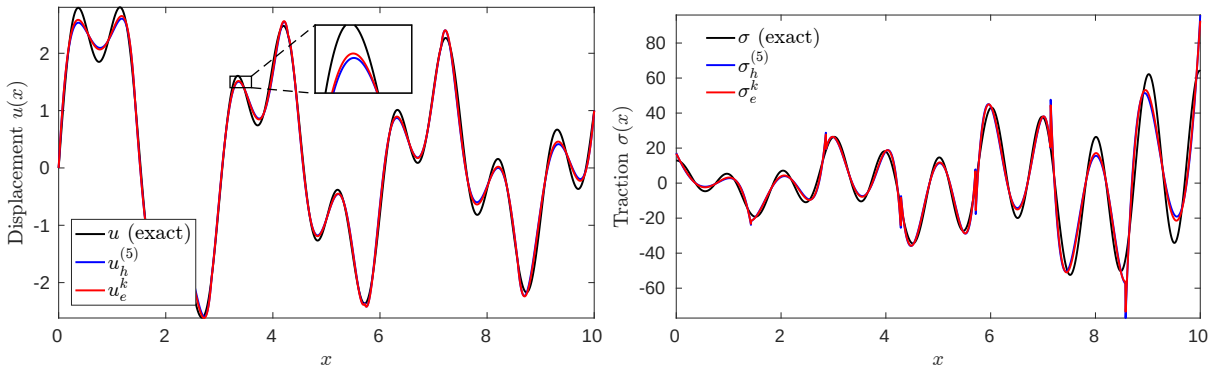

Figure 7: Exact and approximated solutions for the displacement (left) and the traction (right) in a bar with quadratic profile for $k = 2$, an oscillating density of forces with $k_P = \pi k$ and $N = 7$ elements. The resolution is $\lambda/h \approx 2.2$.

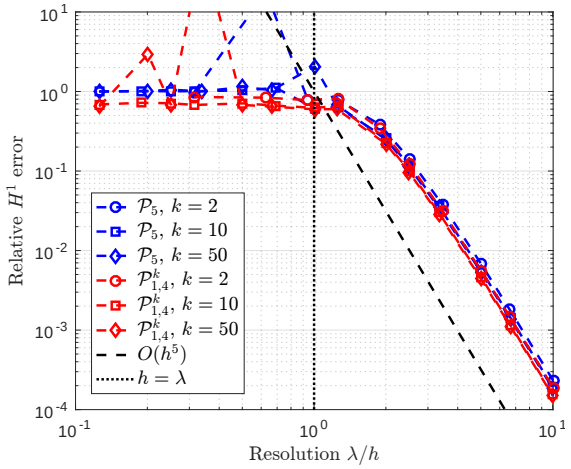

Figure 8: Convergence of solutions using the polynomial space $\mathcal{P}_5$ (blue) and the enriched space $\mathcal{P}_{1,4}^k$ (red), for several wavenumbers, when an oscillating force density is applied.

solutions, then we explain how we build the enriched spaces, and we finally present numerical illustrations of the improvement brought by this additional enrichment.

4.1. Analytical solution for exponential profiles

Recalling that $\mathcal{A} > 0$, the equation (2) can equivalently be written for $f = 0$:

$$-u'' - \frac{\mathcal{A}'}{\mathcal{A}}u' - k^2 u = 0. \tag{24}$$

For any geometrical inhomogeneity, the ratio $\mathcal{A}'/\mathcal{A}$ is therefore the only variable parameter in this equation. In particular, the only possibilities for u to satisfy an ordinary differential equation with constant coefficients are (i) the case of constant profile, in which case (24) reduces to the Helmholtz equation $-u'' - k^2 u = 0$, and (ii) an exponential profile $\mathcal{A} = \mathcal{A}_\delta$ with:

$$\mathcal{A}_\delta(x) = \mathcal{A}_0 e^{2\delta x}, \tag{25}$$

where $1/2\delta$ is the characteristic length of the exponential variation (the factor 2 in its definition will simplify upcoming computations). Note that the case of a constant profile is embedded into the family parametrized by δ, as it corresponds to $\delta = 0$.

We call u_δ the solution of equation (24) with $\mathcal{A} = \mathcal{A}_\delta$, *i.e.* $-u_\delta'' - 2\delta u_\delta' - k^2 u_\delta = 0$, which is written:

$$u_\delta(x) = e^{-\delta x}\left(c_1 \sin\left(\widetilde{k}x\right) + c_2 \cos\left(\widetilde{k}x\right)\right) \qquad \text{with} \qquad \widetilde{k} = \sqrt{k^2 - \delta^2}, \tag{26}$$

where (c_1, c_2) are two real constants.

Remark 5. *Since we focus on high-frequency regimes, we chose to express the solution in terms of sines and cosines, as in the previous section, but for* $|\delta| > k$, i.e. *for low-frequency regimes or very stiff profiles,* $\widetilde{k}$ *is imaginary and the solution* u_δ *is purely exponential. The latter case could be easily handled by setting* $\widetilde{k} = \sqrt{\delta^2 - k^2}$ *and replacing sines and cosines in* (26) *and thereafter by their hyperbolic counterparts.*

4.2. Locally enriched spaces

From a given geometrical parameter δ, we use the basis of solutions (26) as an enrichment family:

$$\Psi^{k,\delta} = \left\{e^{-\delta x}\sin\left(\widetilde{k}x\right), e^{-\delta x}\cos\left(\widetilde{k}x\right)\right\} \quad \text{with} \quad \widetilde{k} = \sqrt{k^2 - \delta^2}. \tag{27}$$

Still leaning on the "half-hat" PU, the corresponding enriched basis, noted $\mathbb{P}^{k,\delta}_{1,4}$, is built by repeating the steps of the previous section 3.1. Additional functions $\widetilde{\varphi}_n^{m\pm}$ are defined similarly to (16) by:

$$\begin{aligned}
\widetilde{\varphi}_n^{1\pm}(x;\delta) &= \varphi_n^{\pm}(x) e^{-\delta(x-x_n)} \sin\left(\widetilde{k}(x-x_n)\right), \\
\widetilde{\varphi}_n^{2\pm}(x;\delta) &= \varphi_n^{\pm}(x) \left(e^{-\delta(x-x_n)} \cos\left(\widetilde{k}(x-x_n)\right) - 1\right).
\end{aligned} \tag{28}$$

Figure 9 represents some of these functions for different parameters δ.

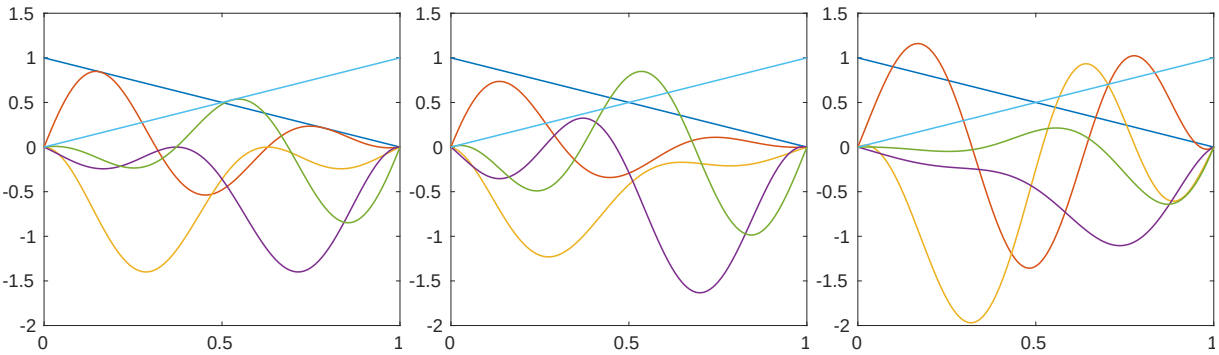

Figure 9: Shape functions of the exponential-enriched basis $\mathbb{P}^{k,\delta}_{1,4}$ on an element of length $h = 1$ and for $k = 10$. From left to right, $\delta = 0$ (sine-enriched basis), $\delta = 1$ and $\delta = -2$.

Following *e.g.* [27], we can eventually build *locally* enriched spaces from sets of parameters $\{\delta_n\}_{n=1\dots N}$. Each of the δ_n is associated with an element I_n and is used to define the elementary enriched basis $\mathbb{P}^{k,\delta_n}_{1,4}$. By analogy with (17), the resulting space, noted $\mathcal{P}^{k,\delta}_{1,4}$, is then the set of functions u_h^δ of the form:

$$u_h^\delta = \sum_{n=0}^{N} u_n^0 \varphi_n^0 + \sum_{n=1}^{N}\sum_{m=1}^{2}\left[u_{n-1}^{m+}\widetilde{\varphi}_{n-1}^{m+}(\cdot;\delta_n) + u_n^{m-}\widetilde{\varphi}_n^{m-}(\cdot;\delta_n)\right]. \tag{29}$$

Quite importantly, these spaces have the same interpolation properties than $\mathcal{P}^k_{1,4}$ (which corresponds to the special case $\delta_n = 0,\ \forall n \in \{1\dots N\}$):

Theorem 3. *The exponential-enriched spaces* $\mathcal{P}^{k,\delta}_{1,4}$*, built from meshes* $\{x_0, \dots, x_N\}$ *and sets* $\{\delta_n\}_{n=0\dots N}$ *of real parameters as described above, satisfy the interpolation property of Theorem 2, with the minor difference that the constant* C_u *now depends also on the chosen set* $\{\delta_n\}_{n=0\dots N}$*.*

The proof of this theorem being very close to the one of Theorem 2 (given in Appendix C), we only underlined the key changes in Appendix D.

Eventually, note that these new spaces have all the implementation-related properties discussed in the previous section 3.2, and in particular static condensation can be applied.

4.3. Choice of the local enrichment

A set $\{\delta_n\}_{n=1...N}$ adapted to our problem, and the corresponding enriched space, are defined by requiring that the functions of the enrichment family Ψ^{k,δ_n} (27) are approximate solutions of the homogeneous Webster's equation (24) in each element I_n. We therefore choose:

$$\delta_n = \frac{1}{2}\frac{\mathcal{A}'(x_{n-1/2})}{\mathcal{A}(x_{n-1/2})}, \tag{30}$$

where $x_{n-1/2}$ is the center of the element I_n. In this way, the enrichment functions satisfy (24) at $x = x_{n-1/2}$, taken as a relation which links their values and those of their derivatives.

When $\mathcal{A}'$ is not known analytically, *e.g.* if $\mathcal{A}$ is given as a set of points rather than a function, approximations of the definition (30) of δ_n can be used, *e.g.*

$$\delta_n \approx \frac{1}{2}\frac{\mathcal{A}(x_n) - \mathcal{A}(x_{n-1})}{h_n \mathcal{A}(x_{n-1/2})}. \tag{31}$$

Geometrically, this enrichment may be seen as an approximation of the profile $\mathcal{A}$ by a piecewise-exponential profile, while the uniform enrichment of the previous section would correspond to a piecewise-constant profile.

Remark 6. *With reference to [20, 28], our choices of enrichment families and set of parameters may also be justified as follows: (i) approximate the relevant variable coefficient of Webster's equation (which is here $\mathcal{A}'/\mathcal{A}$ and not $\mathcal{A}$) by its 0-th order Taylor expansion in each element, and (ii) enrich the FE space with the basis of solutions to the obtained approximated equation.*

4.4. Numerical illustrations

To determine the advantages of the exponential-enriched space, we first compare the convergence behaviors of solutions for three simple profiles. We then address a more complex, multi-domain profile. In all cases, we still consider only clamped–clamped bars (8) with $u_\star = 1$. Since the influence of an oscillating force has already been studied for the sine-enriched space, we keep $f = 0$ in this part. Hereinafter, the locally enriched solution is noted $u_e^{k,\delta}$.

Convex versus concave profiles. Since the enrichment that we propose is geometrically interpreted as a local approximation by a convex exponential profile, we asked ourselves the question of its efficiency for convex or concave profiles, compared to the sine-enriched space corresponding to a constant profile. We therefore compute the approximated solutions in a mono-domain bar of length $L = 10$ for three profiles: quadratic, linear and sinusoidal. For the sinusoidal profile $\mathcal{A}(x) = \mathcal{A}_0 \sin^2(ax + b)$, we impose $ax + b \in [\pi/4, \pi/2]$ for the profile to be concave everywhere, then set $\mathcal{A}_0 = 2$, and finally require that $\mathcal{A}(0) = 1$ and $\mathcal{A}(L) = 2$ to define the other profiles, as specified in Figure 10.

The associated H^1 errors are plotted in Figure 11. On these examples, the exponential-enriched solution follows closely the behavior of the sine-enriched one, with a better precision in the convergence regime in all cases. More precisely, in this convergence regime, we observe a fixed ratio between the numerical errors, *i.e.* there exists a profile-dependent multiplicative constant $C_\mathcal{A}$ such that:

$$E(u_e^{k,\delta}) \approx C_\mathcal{A} E(u_e^k) \text{ for } h > h_0, \text{ with } 0 < C_\mathcal{A} < 1. \tag{32}$$

As expected from the geometrical interpretation of the enrichment, the best improvement is obtained for the convex quadratic profile: we measure $C_\mathcal{A} \approx 0.5$ for the quadratic profile, $C_\mathcal{A} \approx 0.65$ for the linear profile and $C_\mathcal{A} \approx 0.8$ for the sinusoidal profile.

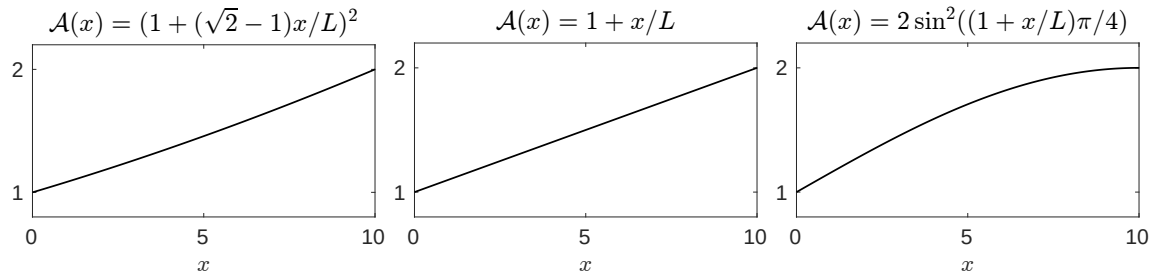

Figure 10: Profiles for mono-domain bars. From left to right, quadratic, linear and sinusoidal profiles.

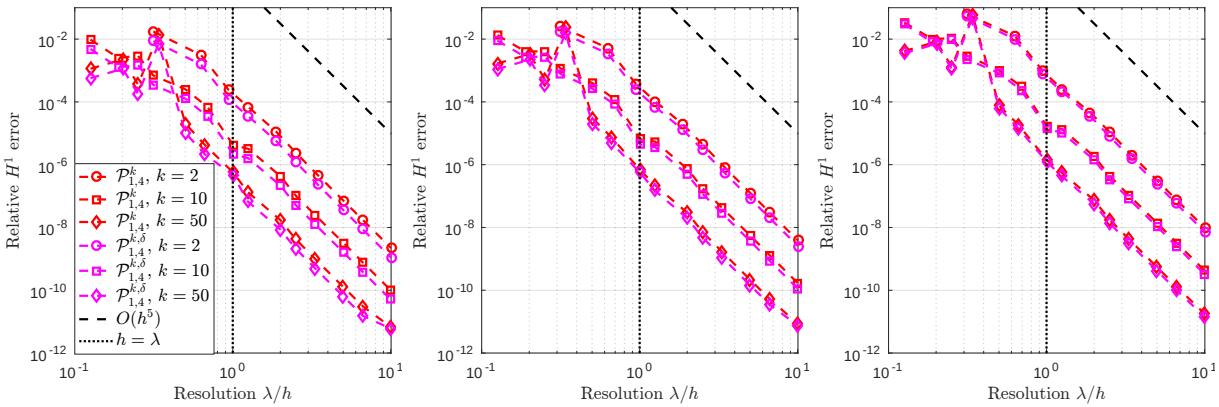

Figure 11: H^1 relative errors associated with quadratic (left), linear (middle) and sinusoidal (right) profiles for sine-enriched (red) and exp-enriched (pink) spaces, and several wavenumbers.

Multidomain bar. For a final illustration, we chose the multidomain configuration represented in Figure 12, in which straight subdomains alternate with stiff quadratic connections. We show in Figure 13 a solution in the particular case of a (cc) bar for low resolution $\lambda/h \approx 0.8$. The exponential-enriched solution is seen to be closer to the exact solution than the sine-enriched solution, and both are better than the polynomial solution, as confirmed by the discrete H^1 errors: one finds $E(u_e^{k,\delta}) = 7.5\%$, while $E(u_e^k) = 18\%$ and $E(u_h^{(5)}) = 66\%$.

In the same configuration, the discrete H^1 error is plotted in Figure 14 for several resolutions and wavenumbers. As expected, the convergence order is the same for all families, while for $k = 2$ we note a quite long transition regime. We retrieve the k-dependent error for fixed resolutions. In all cases, the exponential enrichment brings a clear improvement compared to the previous sine-enriched family, with again a factor $C_{\mathcal{A}} \approx 0.5$ between the two errors.

We underline that the improvement brought by the exponential-enriched space is obtained with almost no additional computational cost compared to the sine-enriched space. Indeed one additionally has to compute the parameters δ_n using (30) or (31), and the basis functions are a bit more involved to evaluate, but theses cost are negligible with respect to the cost of solving the linear systems for large N.

5. Discussion and possible extensions

5.1. On the relevance of high wavenumbers in Webster's equation

For the numerical illustrations in the previous sections, we increased the dimensionless wavenumber until $k = 50$ to show the consistency of our approach at high wavenumbers. However, such wavenumbers are not relevant for many physical phenomena modeled by Webster's equation.

For instance, for the bar model (see Appendix A) the physical wavelength for $k = 50$ would be $\bar{\lambda} = 2\pi r_c/k \approx r_c/10$, *i.e.* the transverse characteristic length r_c would be ten wavelengths long. This

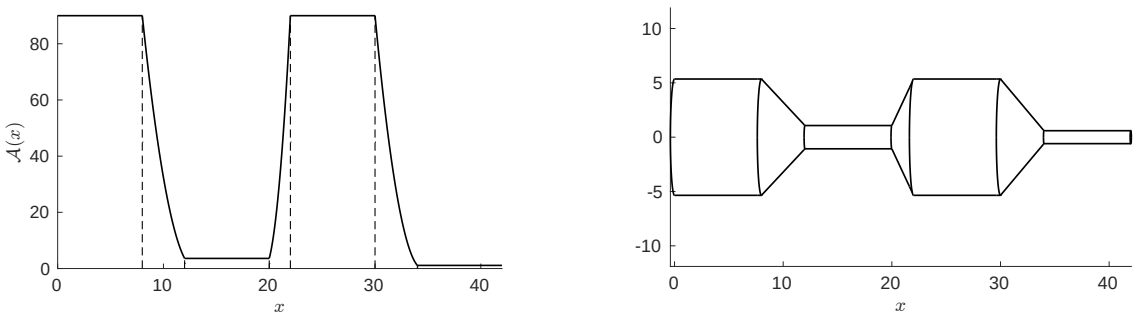

Figure 12: Quadratic-by-parts profile (left) and corresponding bar with circular cross-section and radius $r(x) = \sqrt{\mathcal{A}(x)/\pi}$ (right).

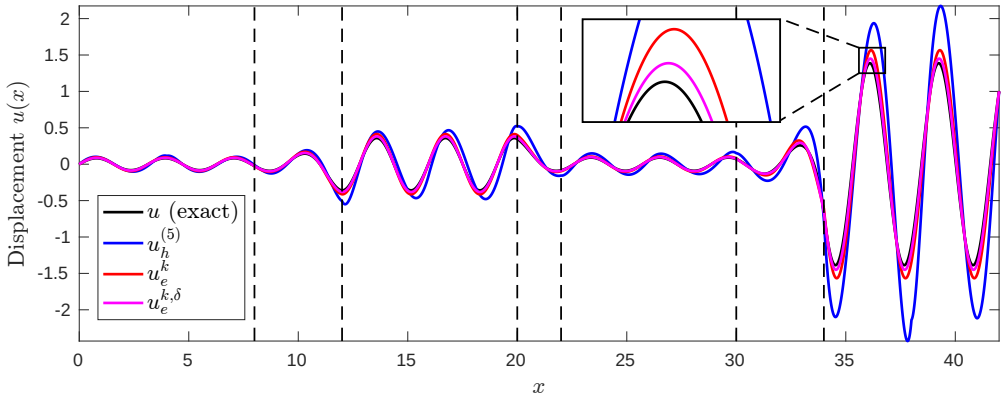

Figure 13: Exact displacement and FE approximations in the multidomain bar for $k = 2$. There are two elements in each straight subdomain, and one in each connection (for a total of $N = 11$ elements), so that $h = \max_n h_n = 4$ and the resolution is $\lambda/h \approx 0.8$.

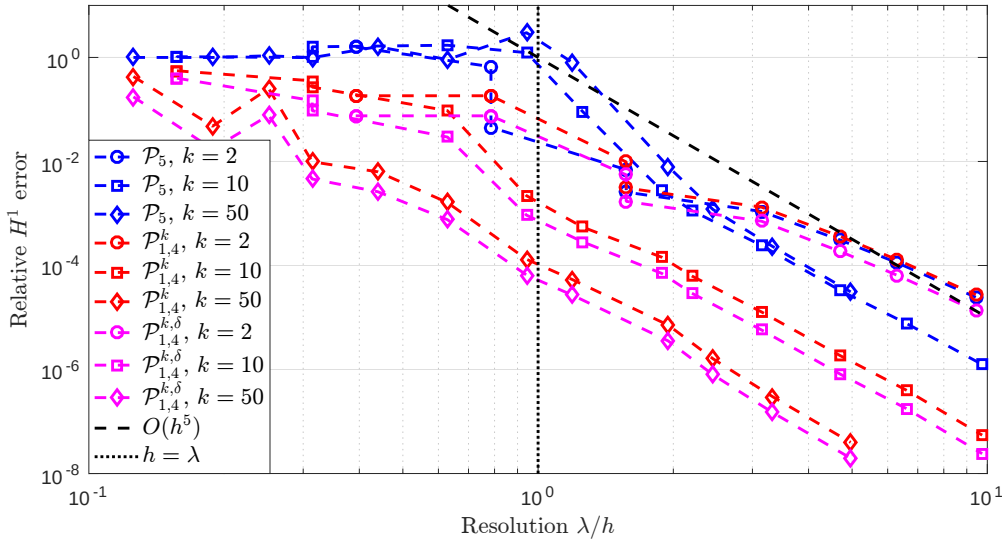

Figure 14: H^1 relative errors for the multidomain bar and for polynomial (blue), sine-enriched (red) and exponential-enriched (magenta) FE spaces, and several wavenumbers.

is significantly too large for the assumptions underlying the 1D bar model to hold, since at such a frequency other vibration modes with transverse direction of propagation are activated inside the structure. Similarly, Webster's equation is derived from three-dimensional problems in ducts and waveguides by [15] and [26] under low-frequency assumptions.

The computations performed for large wavenumbers k must therefore be seen as a proof of concept rather than physically significant simulations.

5.2. Possible choices of geometrical enrichment

Using the exact solutions of Webster's equation for various profiles, given in Appendix A and elsewhere, one can easily use another enrichments than the one corresponding to an exponential profile. The enrichment family $\Psi^{k,\delta}$ (27) should be replaced by the family of solutions corresponding to the chosen profile (*e.g.* Bessel functions for linear profiles $\mathcal{A}_\alpha(x) = \mathcal{A}_0(1+\alpha x)$), and the additional functions (28) should be modified appropriately by ensuring they still vanish at the extremities of the element.

Then, to define the locally enriched space, one should compute a relevant parameter (*e.g.* the slope α for an enrichment corresponding to a linear profile) for each element. Using our criterion, the zeroth-order Taylor expansion of $\mathcal{A}'/\mathcal{A}$ should match with the one of the enrichment profile (*e.g.* α_n should be determined by $\mathcal{A}'_\alpha/\mathcal{A}_\alpha = \alpha_n/(1+\alpha_n x) = \mathcal{A}'/\mathcal{A}$ at $x = x_{n-1/2}$). The implementation of such a space would be exactly the same as the one of the exponential-enriched space, while its interpolation properties would likely depend on the type of profile which is approximated, as we observed in Section 4.4 for the exponential-enriched space.

Following Remark 6, another possible extension is to look for an enrichment profile that matches a higher-order Taylor expansion of $\mathcal{A}'/\mathcal{A}$ in each element, but in this case the enrichment family corresponding to this profile may not be analytical.

5.3. Advantages of the wavenumber-dependent error at fixed resolution

We observed in Figures 5 and 14 that the enriched spaces not only have a convergence threshold h_0 larger than the one of the fifth-order polynomial space, but that the error decreases with the wavenumber k for a given resolution λ/h. In other words, as one increases the wavenumber, a fixed resolution is not needed to keep a given precision. One can even expect to reach the same precision for two computations made at different frequencies while keeping the same mesh size and the same number of basis functions. By comparison, using polynomial spaces $\mathcal{P}_p$ would require to keep the same resolution (*i.e.* a mesh size of $O(k^{-1})$) if the degree p is fixed, or to increase this degree if the mesh size is fixed as described in *e.g.* [25].

From a theoretical point of view, an interesting but possibly quite difficult perspective is the analysis of the above properties, that would support and complete the empirical observations we made in this paper. More precisely, one could focus on (i) the quantification of the threshold associated with the enriched spaces and (iii) the computation of the convergence rate in terms of k for a fixed resolution, that was empirically found to be $O(k^{-2})$ for the quadratic profile studied in Section 3.3 (Figure 5).

From a more computational point of view, this behavior may have major advantages when one has interest in considering several different wavenumbers, or more generally several characteristic lengths for a given problem, which occurs in many situations. Examples of such situations include (i) transient excitation having several components in the frequency domain, for which the solution may be computed by superposition, (ii) force density introducing an additional characteristic length in the problem, as seen in Section 3.3 or (iii) more complex models such as the Timoshenko system for which several wavenumbers intervene simultaneously for each frequency of excitation. Situations (ii) and (iii) are discussed in more detail in the following subsections.

5.4. Extension to higher-order polynomial-enriched spaces

In this paper, we presented spaces $\mathcal{P}_{1,4}$, whose elementary bases are built by adding four internal functions to the $\mathbb{P}_1$ polynomial basis, which results from our choices of using the "half-hat" partition of unity and families of two enrichment functions. By building on this work, it is now easy to define higher-order spaces.

On the one hand, one can increase the order of the initial polynomial basis from 1 to p, by adding the following $p-1$ polynomials from the hierarchical Lobatto basis in the elementary basis. With the enrichment

given in the previous sections, one would obtain a space $\mathcal{P}^{k,\delta}_{p,4}$ which is expected to have the same asymptotic convergence rate than $\mathcal{P}_{p+4}$ in terms of h, while keeping a better convergence threshold and a k-dependent behavior thanks to the enrichment. In other words, we can expect such spaces to combine the advantages of the p-FEM specified in *e.g.* [18, 25] (and notably the exponential convergence as p increases) and the ones described in this paper.

On the other hand, the size of the enrichment family may be increased from 2 to q, by incorporating $2q$ additional functions $\{\varphi^{m\pm}\}_{m=1\dots q}$ in the enriched basis instead of the four functions we used. The first idea that comes to the mind is to use the same kind of enrichment families but with several wavenumbers instead of just one, where the additional "wavenumbers" should be determined from other physical or numerical characteristic lengths. As a simple example, if the "wavenumber" k_{P} corresponding to the characteristic length of the variable force density considered in Section 3.3 was taken into account by adding $\{\sin(k_{\mathrm{P}}x), \cos(k_{\mathrm{P}}x)\}$ to the enrichment family, the particular solution would be embedded in the approximation space. For more complex source term f, approximate solutions of Webster's equation with a suitable local approximation of f may be used to locally enrich elementary bases.

Eventually, these two ideas might be combined to build general spaces $\mathcal{P}_{p,2q}$. For all these spaces, nodal values would still be associated with the $\mathbb{P}_1$ basis functions only (*i.e.* all the other basis functions would be supported by one element only and would vanish at the nodes) and therefore static condensation would be applicable.

5.5. Application to the Timoshenko system

Next, one might wonder if the results of this paper are adaptable to more complex settings and models than the one-dimensional wave equation that we considered.

A natural first step would be to focus on the *transverse* vibrations of thin structures, modeled by the Timoshenko system [12, Sect. 3.4]. As there are very few closed-form analytical solutions to the Timoshenko system when the beam is heterogeneous (see *e.g.* [29] for up-to-date works), obtaining an efficient numerical method may indeed be of significant practical interest. This problem is also one-dimensional in the sense that the fields still depend only on the longitudinal coordinate x, but it features additional key challenges including (i) a coupled system of equations driving the transverse displacement and the section rotation angle, (ii) two relevant variable geometrical parameters (the area of the cross-section and its quadratic momentum) and consequently (iii) two distinct wavenumbers for each frequency of excitation. Note that the point (iii) *a priori* indicates that enriched spaces embedding four enrichment functions should be used, *i.e.* spaces of the type $\mathcal{P}_{p,8}$ with the notation introduced above in Section 5.4.

5.6. About the extension to higher dimensions

Another important extension would be the transposition of our methods to two- or three-dimensional problems. In these cases, the space of solutions to time-harmonic wave equations *e.g.* $-\mathrm{div}(\mathcal{A}\nabla u)-\mathcal{A}k^2u = f$ is of infinite dimension, contrarily to the two-dimensional space of solutions in 1D, whose basis can be approximated with the enrichment families $\Psi^{k,\delta}$ (27). Consequently, we do not expect our arguments to remain valid for any problem, and in particular replacing straightforwardly the PU by its higher-dimensional counterpart and the enrichment families by $\{e^{\pm \mathrm{i}\boldsymbol{k}\cdot\boldsymbol{x}}\}$, with $\boldsymbol{k} = k\boldsymbol{d}$ a given wavevector in the direction $\boldsymbol{d}$, is not expected to produce efficient FE spaces. Indeed, an entire collection of N_{w} plane waves in different directions $\{\boldsymbol{d}_p\}_{p=1\dots N_{\mathrm{w}}}$ must generally be used to capture such a solution when the only *a priori* available information is its wavenumber, see again [23] and the references therein.

We therefore think that our ideas may be applied if one deals with problems that feature a known directionality, or is able to obtain some additional information about relevant enrichment directions in each element. The most classical example of a problem with an intrinsic directionality is the scattering (or the transmission) of a plane wave $e^{\mathrm{i}k\boldsymbol{d}_{\mathrm{i}}\cdot\boldsymbol{x}}$ by an obstacle. In this case, the direction $\boldsymbol{d}_{\mathrm{i}}$ of the incident wave is privileged, and the knowledge of this direction may be used to fasten existing numerical methods designed to solve arbitrary wave problems. As an example among other, let us quote the *microlocal discretization* of [1], which is designed precisely to deal with high-frequency scattering problems by incorporating explicitly the incident wavevector $\boldsymbol{k}_{\mathrm{i}} = k\boldsymbol{d}_{\mathrm{i}}$ in the finite element spaces while using a boundary element method. On

the other hand, for an arbitrary wave problem, the ideas of the microlocal analysis can also be exploited to *extract* a privileged direction from a wavefield at a given points. For instance, the recent work [11], to which we refer for more references on microlocal analysis, builds an enriched finite element space thanks to the information extracted from the solution of a low frequency problem featuring the same propagation medium and source term.

6. Conclusion

In this work, we presented new spaces and corresponding bases of enriched finite elements to deal with one-dimensional time-harmonic wave problems with spatially variable coefficients, modeled with Webster's equation. A first basis embeds the knowledge of the frequency of vibration through a global enrichment by sines and cosines. It is built following the partition of unity method but using "half-hat" functions as the partition of unity, which permits an easy comparison with a classical fifth-order polynomial basis: our basis is implemented identically in the finite element framework and the corresponding solution is proven to have the same convergence rate. Static condensation is possible and therefore the computational cost is close for both bases. Preliminary numerical studies emphasize the large improvement of the convergence threshold brought by our basis, for which convergence begins for low resolutions ($\lambda/h < 1$), and its dependency on the frequency for fixed resolution, so that the solution converges faster at high frequencies.

We then incorporated an additional information on the geometrical heterogeneity and generalized our first basis to a whole family of "exponentially-enriched" bases, that were used to build a locally enriched space. With a very slight increase of the computational cost compared to the previously studied bases, we observed a stable decrease of the error in the convergence regime, up to 50% depending on the nature of the approximated profile.

Some relevant points encountered during the study were finally discussed, along with several possible extensions.

Acknowledgments

The authors acknowledge the support of the Centre Henri Lebesgue ANR-11-LABX-0020-01 provided through a post-doctoral fellowship to R. Cornaggia. They also thank the reviewers for their numerous and relevant comments and corrections.

Appendix A. Webster's equation: derivation for geometrically heterogeneous bars and existing exact solutions

Consider a straight bar made of a homogeneous material characterized by density ρ and Young's modulus E, and whose cross-section has a variable area $A(\bar{x})$ depending on the longitudinal coordinate $\bar{x}$. The quantities of interest are the longitudinal displacement $\bar{u}(\bar{x})$ of the medium axis of the bar, and the traction $\bar{\sigma}(\bar{x})$ applied on the cross-sections, which are linked by the classical linear elastic constitutive relation $\bar{\sigma}(\bar{x}) = EA(d\bar{u}/d\bar{x})(\bar{x})$. When a linear force density $\bar{f}(\bar{x})$ is applied, the equilibrium of the bar is written (see *e.g.* [12, Chap.2]):

$$-\bar{\omega}^2 \rho A \bar{u} = \frac{d}{d\bar{x}}\left(EA\frac{d\bar{u}}{d\bar{x}}\right) + \bar{f}. \tag{A.1}$$

To work with non-dimensional quantities only, we introduce the fixed characteristic cross-section $A_\mathrm{c} > 0$ (which can be *e.g.* $A_\mathrm{c} = A(0)$, or the mean value of A along the bar) and the characteristic radius $r_\mathrm{c} = \sqrt{A_\mathrm{c}}$. Using also the constant longitudinal wavespeed $c = \sqrt{E/\rho}$, we define non-dimensional counterparts of the various parameters and fields used in (A.1):

$$x = \frac{\bar{x}}{r_\mathrm{c}}, \quad u = \frac{\bar{u}}{r_\mathrm{c}}, \quad k = r_\mathrm{c}\frac{\bar{\omega}}{c}, \quad f = \frac{\bar{f}}{Er_\mathrm{c}}, \quad \text{and} \quad \sigma = \frac{\bar{\sigma}}{EA_\mathrm{c}}, \tag{A.2}$$

while the dimensionless counterpart of the cross-section is the strictly positive function $\mathcal{A}$ defined by:

$$A(\bar{x}) = A_{\mathrm{c}}\mathcal{A}(x), \quad \text{that is} \quad \mathcal{A}(x) = A(r_{\mathrm{c}}x)/A_{\mathrm{c}}. \tag{A.3}$$

The constitutive relation becomes $\sigma = \mathcal{A}u'$ and the equilibrium equation (A.1) written in terms of these new variables is Webster's equation:

$$-k^2\mathcal{A}u = (\mathcal{A}u')' + f. \tag{A.4}$$

Analytical solutions of this equation are available in the literature for specific profiles $\mathcal{A}$. Without pretension of exhaustivity, we give here some solutions corresponding to the profiles used in the numerical examples. These solutions were also derived by other authors, see *e.g.* [8] for a historical review of Webster's equation.

Linear profiles $\mathcal{A}(x) = x$ are addressed in [12, Sec. 2.5.1], and the associated solution is given in terms of Bessel functions (J_0, Y_0) or Hankel functions $(H_0^{(1)}, H_0^{(2)})$:

$$u(x) = c_1 J_0(kx) + c_2 Y_0(kx) \quad \text{or} \quad u(x) = c_1 H_0^{(1)}(kx) + c_2 H_0^{(2)}(kx), \quad (c_1, c_2) \in \mathbb{C}^2. \tag{A.5}$$

A more general expression $\mathcal{A}(x) = \mathcal{A}_0(1 + \alpha x)$ with $\alpha \in \mathbb{R}$ is also addressed, in which case one obtains:

$$u(x) = c_1 J_0\left(\frac{k}{\alpha}(1+\alpha x)\right) + c_2 Y_0\left(\frac{k}{\alpha}(1+\alpha x)\right). \tag{A.6}$$

For a *quadratic profile* $\mathcal{A}(x) = x^2$, the wave equation with constant coefficients is also shown in [12] to be satisfied by xu (*i.e.* $(xu)'' + k^2(xu) = 0$), so that the solution basis for u is $\{\cos(kx)/x, \sin(kx)/x\}$. [2] shows that the same approach can be applied to more general profiles of the form $\mathcal{A}(x) = \mathcal{A}_0(1 + \alpha x)^2$, in which case:

$$u(x) = \frac{c_1 \sin(kx) + c_2 \cos(kx)}{1 + \alpha x}. \tag{A.7}$$

Eventually, [22] generalizes these solutions to any profile of the form $\mathcal{A}(x) = \mathcal{A}_0 (1 + \alpha x)^n$ for $n \in \mathbb{R}\backslash\{0\}$. The associated solutions depend on whether the index $m = (1 - n)/2$ is an integer or not, as follows:

$$\begin{aligned} u(x) &= (1+\alpha x)^m \left[c_1 J_m\left(\frac{k}{\alpha}(1+\alpha x)\right) + c_2 Y_m\left(\frac{k}{\alpha}(1+\alpha x)\right)\right] \quad \text{when } m \in \mathbb{Z}, \\ u(x) &= (1+\alpha x)^m \left[c_1 J_m\left(\frac{k}{\alpha}(1+\alpha x)\right) + c_2 J_{-m}\left(\frac{k}{\alpha}(1+\alpha x)\right)\right] \quad \text{when } m \notin \mathbb{Z}. \end{aligned} \tag{A.8}$$

They also deal with *sinusoidal profiles* $\mathcal{A}(x) = \mathcal{A}_0 \sin^2(ax + b)$. Using the change of unknown $y(x) = u(x)\sin(ax + b)$, one finds that $y'' + (k^2 + a^2)y = 0$, and therefore:

$$u(x) = \frac{c_1 \sin(\hat{k}x) + c_2 \cos(\hat{k}x)}{\sin(ax + b)}, \quad \text{with } \hat{k} = \sqrt{k^2 + a^2}. \tag{A.9}$$

For completeness, we also note that general polynomial profiles (not limited to powers of $(1 + \alpha x)$) are addressed in [7], but in this case the displacement is less conveniently expressed as an infinite polynomial expansion whose coefficients satisfy recurrence relations.

Finally, for a bar that can be decomposed into subdomains whose cross-section areas have the above profiles, and still when $f = 0$, the solution is obtained by (i) writing the displacement u as a linear combination of the two functions of the basis corresponding to the current profile in each subdomain, (ii) enforcing the transmission conditions (displacement and traction continuity) at each interface between two subdomains and (iii) enforcing the boundary conditions.

Appendix B. Hierarchical basis of Lobatto polynomials

Using the notation of [17, Sec. 4.7], the Lobatto basis functions for p-th order polynomial elements are defined on a reference element $[-1, 1]$ as:

$$N_1(\zeta) = \frac{1-\zeta}{2}, \quad N_l(\zeta) = \sqrt{\frac{2l-1}{2}} \int_{-1}^{\zeta} P_{l-1}(t)dt \quad \text{for } l = 2 \dots p, \quad \text{and} \quad N_{p+1}(\zeta) = \frac{1+\zeta}{2}, \tag{B.1}$$

where N_1 and N_{p+1} are the restrictions of hat functions to the element and the $\{N_l\}_{l=2\dots p}$ are the Lobatto polynomials, defined from the Legendre polynomials P_n. Their explicit expressions up to $l = 5$ are:

$$\begin{aligned}
P_1(t) &= t, & N_2(\zeta) &= \frac{\sqrt{6}}{4}(\zeta^2-1),\\
P_2(t) &= \frac{1}{2}(3t^2-1), & N_3(\zeta) &= \frac{\sqrt{10}}{4}\zeta(\zeta^2-1),\\
P_3(t) &= \frac{1}{2}(5t^3-3t), & N_4(\zeta) &= \frac{\sqrt{14}}{16}(\zeta^2-1)(5\zeta^2-1),\\
P_4(t) &= \frac{1}{8}(35t^4-30t^2+3), & N_5(\zeta) &= \frac{3\sqrt{2}}{16}\zeta(\zeta^2-1)(7\zeta^2-3).
\end{aligned} \tag{B.2}$$

In our case, the reference element is $[0, 1]$, so the definition of basis functions includes the additional change of variable $\zeta = 2\xi - 1$, $\xi \in [0, 1]$.

Appendix C. Proof of Theorem 2

As often, the proof is constructive: given an arbitrary function u continuous on $[0, L]$ and such that $u_{|I_n} \in C^6(I_n)$ for all the elements I_n, we will build an approximation $w_h \in \mathcal{P}^k_{1,4}$ of u that satisfies the same inequalities than the infimum of equation (19) but with a different constant C_u. We first (i) specify our choice of w_h, then (ii) study the elementary error associated with this choice and finally (iii) conclude by summing these errors on all the elements. In this proof, the C_j, with $j \in \mathbb{N}^*$, denote positive constants whose precise evaluation is not needed.

(i) Construction of w_h: first recall from (17) that w_h is written:

$$w_h = \sum_{n=0}^{N} w_n^0 \varphi_n^0 + \sum_{n=1}^{N} \sum_{m=1}^{2} \left(w_{n-1}^{m+} \varphi_{n-1}^{m+} + w_n^{m-} \varphi_n^{m-} \right). \tag{C.1}$$

Our first requirement is quite intuitive: w_h should interpolate u at each node x_n, *i.e.*

$$w_h(x_n) = w_n^0 = u(x_n). \tag{C.2}$$

Four degrees of freedom per element I_n are yet to be determined, corresponding to the internal functions $[\varphi_n^{1-}, \varphi_{n-1}^{1+}, \varphi_n^{2-}, \varphi_{n-1}^{2+}]$. To lighten a bit the notation, we focus on an element I_n in which we note $W = [w^{1-}\ w^{1+}\ w^{2-}\ w^{2+}]^{\mathrm{T}}$ the vector of internal values. We also note $\tilde{u}$ and $\tilde{w}$ the restrictions of u and w_h to I_n, taken as functions of the scaled variable $\xi = (x - x_{n-1})/h_n \in [0, 1]$:

$$\begin{aligned}
&\tilde{u}(\xi) = u(x_{n-1} + h_n\xi),\\
&\tilde{w}(\xi) = (1-\xi)\tilde{u}(0) + \xi\tilde{u}(1) + \left[w^{1-}\varphi^{1-} + w^{1+}\varphi^{1+} + w^{2-}\varphi^{2-} + w^{2+}\varphi^{2+} \right](\xi; k, h_n),
\end{aligned} \tag{C.3}$$

where the node interpolation requirement is included in the definition of $\tilde{w}$ and translates into $\tilde{u}(0) = \tilde{w}(0)$ and $\tilde{u}(1) = \tilde{w}(1)$, and the internal functions (also expressed in terms of ξ) are:

$$\begin{aligned}
\varphi^{1-}(\xi; k, h) &= \xi \sin(kh(\xi-1)), & \varphi^{1+}(\xi; k, h) &= (1-\xi)\sin(kh\xi),\\
\varphi^{2-}(\xi; k, h) &= \xi\left(\cos(kh(\xi-1)) - 1\right), & \varphi^{2+}(\xi; k, h) &= (1-\xi)\left(\cos(kh\xi) - 1\right).
\end{aligned} \tag{C.4}$$

Pursuing our construction of the local approximation $\tilde{w}$, the internal values gathered in W are fixed by imposing the equality of the derivatives of $\tilde{u}$ and $\tilde{w}$ at $\xi = 0$, up to the fourth derivative, *i.e.* $\tilde{w}^{(p)}(0) = \tilde{u}^{(p)}(0),\ p = 1 \dots 4$. This is written as the linear system:

$$M \cdot W = U, \quad \text{with} \quad M = \begin{bmatrix} -s & \beta & c-1 & 0 \\ 2c & -2 & 2s & -\beta \\ 3s & -\beta & -3c & 3 \\ -4c & 4 & -4s & \beta \end{bmatrix} \quad \text{and} \quad U = \begin{bmatrix} \tilde{u}'(0) - (\tilde{u}(1) - \tilde{u}(0)) \\ \tilde{u}''(0)/\beta \\ \tilde{u}^{(3)}(0)/\beta^2 \\ \tilde{u}^{(4)}(0)/\beta^3 \end{bmatrix}. \tag{C.5}$$

where we used the notations $\beta = kh_n$, $c = \cos\beta$ and $s = \sin\beta$ for compactness. The matrix M is always invertible, as its determinant $\det(M) = \beta(6\sin\beta - \beta(2\cos\beta + 4))$ is strictly negative for any $\beta > 0$. Therefore, W and $\tilde{w}$ are uniquely determined by (C.5).

(ii) Evaluation of the elementary error: we then focus on the error $e := \tilde{u} - \tilde{w}$. As $e^{(p)}(0) = 0$ for $p = 0 \dots 4$ by construction, we have, using Taylor expansions with integral remainders:

$$e(\xi) = e^{(5)}(0)\frac{\xi^5}{5!} + \int_0^\xi \frac{e^{(6)}(t)}{5!}(\xi - t)^5 \, \mathrm{d}t \qquad \text{and} \qquad e'(\xi) = e^{(5)}(0)\frac{\xi^4}{4!} + \int_0^\xi \frac{e^{(6)}(t)}{4!}(\xi - t)^4 \, \mathrm{d}t. \tag{C.6}$$

Moreover, we have $e(1) = 0$ (still by construction). We can therefore compute $e^{(5)}(0)$ by setting $\xi = 1$ in the expression of $e(\xi)$ given above, then express $e'(\xi)$ using only the sixth derivative $e^{(6)}$ as:

$$e'(\xi) = \frac{1}{4!}\left[-\left(\int_0^1 e^{(6)}(t)(1-t)^5 \, \mathrm{d}t \right) \xi^4 + \int_0^\xi e^{(6)}(t)(\xi - t)^4 \, \mathrm{d}t \right]. \tag{C.7}$$

Finally, we can bound $|e'(\xi)|$ in $[0, 1]$ by:

$$\begin{aligned} |e'(\xi)| &\le \frac{1}{4!}\left[\left(\int_0^1 \left| e^{(6)}(t)(1-t)^5 \right| \, \mathrm{d}t \right) \xi^4 + \int_0^\xi \left| e^{(6)}(t)(\xi - t)^4 \right| \, \mathrm{d}t \right] \\ &\le \frac{1}{4!}\left[\int_0^1 \left| e^{(6)}(t)(1-t)^5 \right| \, \mathrm{d}t + \int_0^1 \left| e^{(6)}(t)(\xi - t)^4 \right| \, \mathrm{d}t \right] && \text{(because } \xi^4 \le 1\text{)} \\ &\le \frac{1}{4!}\left[C_1 \|e^{(6)}\|_{L^2(0,1)} + C_2 \|e^{(6)}\|_{L^2(0,1)} \right] && \text{(using Cauchy–Schwarz inequalities)} \\ &\le \frac{C_1 + C_2}{4!} \|e^{(6)}\|_{L^2(0,1)}. \end{aligned} \tag{C.8}$$

Consequently, we have $\|e'\|^2_{L^2(0,1)} \le C_3 \|e^{(6)}\|^2_{L^2(0,1)}$. Coming back to the functions u and w_h, *i.e.* after the change of variable $x = x_{n-1} + h_n\xi$, this inequality translates into:

$$\|u' - w_h'\|^2_{L^2(I_n)} \le C_3 h_n^{10} \|u^{(6)} - w_h^{(6)}\|^2_{L^2(I_n)}. \tag{C.9}$$

Since $(u - w_h)(x_{n-1}) = 0$ we can apply the Poincaré inequality in I_n to evaluate the L^2 error:

$$\|u - w_h\|^2_{L^2(I_n)} \le h_n^2 \|u' - w_h'\|^2_{L^2(I_n)} \le C_3 h_n^{12} \|u^{(6)} - w_h^{(6)}\|^2_{L^2(I_n)}. \tag{C.10}$$

We now need to work on the norm $\|u^{(6)} - w_h^{(6)}\|^2_{L^2(I_n)}$ to study its dependency on h_n. We begin by the decomposition:

$$\begin{aligned} \|u^{(6)} - w_h^{(6)}\|^2_{L^2(I_n)} &\le \|u^{(6)}\|^2_{L^2(I_n)} + \|w_h^{(6)}\|^2_{L^2(I_n)} + 2\|u^{(6)}\|_{L^2(I_n)} \|w_h^{(6)}\|_{L^2(I_n)} \\ &\le \|u^{(6)}\|^2_{L^2(I_n)} + \|w_h^{(6)}\|^2_{L^2(I_n)} + 2h_n^{1/2} \max_{x \in I_n} \left| u^{(6)}(x) \right| \|w_h^{(6)}\|_{L^2(I_n)}. \end{aligned} \tag{C.11}$$

The norm $\|w_h^{(6)}\|_{L^2(I_n)}$ deserves attention, as $w_{h|I_n}$ is defined through the inversion of the linear system (C.5), in which h_n appears both in the matrix M and the right-hand side U. We solved this system using the symbolic calculus software Maple, collected the leading-order terms arising from the product $M^{-1}U$ (using the Taylor expansion of the first term of U when necessary), and found:

$$\begin{aligned}
w^{1-} &= -\frac{1}{2}\left(3\frac{u^{(5)}(x_{n-1})}{k^5}+5\frac{u^{(3)}(x_{n-1})}{k^3}\right)+\frac{5}{4}\frac{u''(x_{n-1})}{k^2}h_n+O(h_n^2),\\
w^{1+} &= -\frac{1}{2}\left(3\frac{u^{(5)}(x_{n-1})}{k^5}+5\frac{u^{(3)}(x_{n-1})}{k^3}\right)-\frac{1}{4}\left(2\frac{u^{(4)}(x_{n-1})}{k^3}+\frac{u''(x_{n-1})}{k}\right)h_n+O(h_n^2),\\
w^{2-} &= -\frac{u^{(4)}(x_{n-1})}{k^4}-2\frac{u''(x_{n-1})}{k^2}-\left(\frac{u^{(5)}(x_{n-1})}{k^4}+2\frac{u^{(3)}(x_{n-1})}{k^2}\right)h_n+O(h_n^2),\\
w^{2+} &= -\frac{u^{(4)}(x_{n-1})}{k^4}-2\frac{u''(x_{n-1})}{k^2}.
\end{aligned} \tag{C.12}$$

Computing the L^2-norm of $w_h^{(6)}$ finally gives:

$$\begin{aligned}
\|w_h^{(6)}\|_{L^2(I_n)} &= h_n^{1/2}F_u(x_{n-1})+O(h_n) \qquad \text{with} \quad F_u(x) := k^2\left|k^2u''(x)+2u^{(4)}(x)\right|\\
&\le C_4 h_n^{1/2}F_u(x_{n-1}) \qquad\qquad \text{for any } C_4>1 \text{ and } h_n \text{ small enough,}
\end{aligned} \tag{C.13}$$

and (C.11) becomes:

$$\|u^{(6)}-w_h^{(6)}\|^2_{L^2(I_n)} \le \|u^{(6)}\|^2_{L^2(I_n)} + C_4^2 h_n\left[F_u(x_{n-1})\left(F_u(x_{n-1})+2\max_{x\in I_n}\left|u^{(6)}(x)\right|\right)\right] \text{ for } h_n \text{ small enough.} \tag{C.14}$$

(iii) Conclusion on the whole domain: summing the inequality (C.9) over all the elements, one obtains

$$\sum_{n=1}^{N}\|u'-w_h'\|^2_{L^2(I_n)} \le C_5 h^{10}\left\{LD_u+\sum_{n=1}^{N}\|u^{(6)}\|^2_{L^2(I_n)}\right\} \text{ for } h \text{ small enough,} \tag{C.15}$$

where $h := \max_n h_n$ and $D_u := \max_{x\in\cup_n I_n} F_u(x)\left(F_u(x)+2\left|u^{(6)}(x)\right|\right)$ depends only on u. A similar inequality for the L^2 misfit, but with h^{12} instead of h^{10}, is obtained in the same way by summing the inequality (C.10). Finally, Theorem 2 is proven by taking the square roots of these inequalities, and then claiming that the error reached by taking the unknown best interpolant in $\mathcal{P}^k_{1,4}$ is inferior to the one obtained above with a specific choice of w_h.

Remark 7. *The assumption $u \in C^6(I_n)$ rather than $u \in H^6(I_n)$, apart from its physical relevance discussed after Theorem 2, comes from the need to evaluate $\|w_h^{(6)}\|_{L^2(I_n)}$. More precisely, it intervened in* (C.11) *where replacing the estimate $\|u^{(6)}\|_{L^2(I_n)} < h_n^{1/2}\max_{x\in I_n}\left|u^{(6)}(x)\right|$ by just $\|u^{(6)}\|_{L^2(I_n)} < C$ for some $C>0$ would have caused the lost of a half-order in the final result.*

Remark 8. *Our choice for the construction of w_h, which implied "asymmetric" requirements (equality of derivatives at left end of each element), was made to simplify the ensuing computations, and notably the Taylor expansions* (C.6)*. It is certainly not optimal, in the sense that the bracketed term in* (C.15) *does not provide the optimal constant C_u that appears in Theorem 2.*

Appendix D. Elements of proof of Theorem 3

We provide here the main changes compared to the proof for the sine-enriched space, and check that the key steps are still valid. The internal additional functions of the enriched basis are:

$$\begin{aligned}
\widetilde{\varphi}^{1-}(\xi;k,\delta,h) &= \xi e^{-\delta h(\xi-1)}\sin\left(\widetilde{k}h(\xi-1)\right),\\
\widetilde{\varphi}^{1+}(\xi;k,\delta,h) &= (1-\xi)e^{-\delta h\xi}\sin\left(\widetilde{k}h\xi\right),\\
\widetilde{\varphi}^{2-}(\xi;k,\delta,h) &= \xi\left(e^{-\delta h(\xi-1)}\cos\left(\widetilde{k}h(\xi-1)\right)-1\right),\\
\widetilde{\varphi}^{2+}(\xi;k,\delta,h) &= (1-\xi)\left(e^{-\delta h\xi}\cos\left(\widetilde{k}h\xi\right)-1\right).
\end{aligned} \tag{D.1}$$

The matrix $\tilde{M}$ and RHS $\tilde{U}$ arising form the requirement of equal derivatives at $\xi = 0$ are defined similarly to (C.5), except that the lines of $\tilde{M}$ are not homogeneous in $\tilde{\beta} := \widetilde{k}h_n$ anymore and therefore $\tilde{U}_j = \tilde{u}^{(j)}$ for $j = 2\dots 4$ (no division by $\tilde{\beta}^{j-1}$). In particular, the determinant of $\tilde{M}$ is:

$$\begin{aligned}
&\tilde{D}(\tilde{\beta},d) = -2e^d(d^2+\tilde{\beta}^2)\tilde{\beta}\\
&\times\left(2\tilde{\beta}^3e^d\left[\tilde{\beta}^2+d^2-4d\right]+\tilde{\beta}\cos(\tilde{\beta})\left[\tilde{\beta}^4+8d\tilde{\beta}^2-d^4\right]+\sin(\tilde{\beta})\left[\tilde{\beta}^4(2d-3)+2\tilde{\beta}^2d^2(3+d)+d^4\right]\right),
\end{aligned} \tag{D.2}$$

where $d = \delta h_n$. This time, this determinant is not always sign-definite, in particular it might oscillate when $\delta < 0$ and $\tilde{\beta}$ varies. This is not surprising, as the sign of δ introduces a "directionality" in the enriched basis that does not exist for polynomial or sine-enriched bases. For the proof to remain valid we therefore introduce an additional requirement: *when $\delta_n < 0$, the equality of derivatives must be imposed at $\xi = 1$ rather than $\xi = 0$.* In this case, by the change of variable $\tilde{\xi} = 1-\xi$ and thanks to the symmetry of the basis functions (D.1), one sees that we obtain a system identical to the one obtained for $\delta > 0$.

Finally, after solving the linear system, we checked that the estimate (C.13) of $\|w_h^{(6)}\|_{L^2(I_n)}$ still holds, *i.e.* that $\|w_h^{(6)}\|_{L^2(I_n)} = (h_n)^{1/2}\tilde{F}_u + O(h_n)$ for some function $\tilde{F}_u$ that does not depend on h_n.

References

[1] T. Abboud, J.-C. Nédélec, and B. Zhou. Improvement of the integral equation method for high frequency problems. In *Third international conference on mathematical aspects of wave propagation phenomena, SIAM*, pages 178–187, 1995.

[2] S. Abrate. Vibration of non-uniform rods and beams. *Journal of Sound and Vibration*, 185(4):703 – 716, 1995.

[3] M. Arndt, R. Machado, and A. Scremin. An adaptive generalized finite element method applied to free vibration analysis of straight bars and trusses. *Journal of Sound and Vibration*, 329(6):659 – 672, 2010.

[4] A. K. Aziz, R. B. Kellogg, and A. B. Stephens. A two point boundary value problem with a rapidly oscillating solution. *Numerische Mathematik*, 53(1):107–121, Jan 1988.

[5] P. Ciarlet Jr. T-coercivity: Application to the discretization of Helmholtz-like problems. *Computers & Mathematics with Applications*, 64(1):22 – 34, 2012.

[6] L. Demkowicz. Asymptotic convergence in finite and boundary element methods: part 1: theoretical results. *Computers & Mathematics with Applications*, 27(12):69 – 84, 1994.

[7] M. Eisenberger. Exact longitudinal vibration frequencies of a variable cross-section rod. *Applied Acoustics*, 34(2):123 – 130, 1991.

[8] E. Eisner. Complete solutions of the "Webster" horn equation. *The Journal of the Acoustical Society of America*, 41(4B):1126–1146, 1967.

[9] A. Ern and J.-L. Guermond. *Theory and practice of finite elements*, volume 159. Springer Science & Business Media, 2004.

[10] S. Esterhazy and J. Melenk. On stability of discretizations of the Helmholtz equation (extended version). Technical report, Inst. for Analysis and Sci. Computing, of Technology, Vienna Univ., 2011. Available at http://www.asc.tuwien.ac.at and arXiv:1105.2112.

[11] J. Fang, J. Qian, L. Zepeda-Núñez, and H. Zhao. Learning dominant wave directions for plane wave methods for high-frequency Helmholtz equations. *Research in the Mathematical Sciences*, 4(1):9, May 2017.

[12] K. F. Graff. *Wave motion in elastic solids*. Oxford University Press, 1975.

[13] I. G. Graham and S. A. Sauter. Stability and error analysis for the Helmholtz equation with variable coefficients. *ArXiv e-prints*, Mar. 2018. arXiv:1803.00966.

[14] S. Ham and K.-J. Bathe. A finite element method enriched for wave propagation problems. *Computers & Structures*, 94-95:1 – 12, 2012.
[15] T. Hélie. Unidimensional models of acoustic propagation in axisymmetric waveguides. *The Journal of the Acoustical Society of America*, 114(5):2633–2647, 2003.
[16] R. Hiptmair, A. Moiola, and I. Perugia. *A Survey of Trefftz Methods for the Helmholtz Equation*, pages 237–279. Springer International Publishing, Cham, 2016.
[17] F. Ihlenburg. *Finite Element Analysis of Acoustic Scattering*. Springer Publishing Company, Incorporated, 1998.
[18] F. Ihlenburg and I. Babuška. Finite element solution of the Helmholtz equation with high wave number part II: The h-p version of the FEM. *SIAM Journal on Numerical Analysis*, 34(1):315–358, 1997.
[19] F. Ihlenburg and I. Babuška. Solution of Helmholtz problems by knowledge-based FEM. *Computer Assisted Mechanics and Engineering Sciences*, pages 397–415, 1997.
[20] L.-M. Imbert-Gérard and B. Després. A generalized plane-wave numerical method for smooth nonconstant coefficients. *IMA Journal of Numerical Analysis*, 34(3):1072–1103, 2014.
[21] H. Kohno, K.-J. Bathe, and J. C. Wright. A finite element procedure for multiscale wave equations with application to plasma waves. *Computers & Structures*, 88(1-2):87 – 94, 2010.
[22] B. Kumar and R. Sujith. Exact solutions for the longitudinal vibration of non-uniform rods. *Journal of Sound and Vibration*, 207(5):721 – 729, 1997.
[23] A. Lieu, G. Gabard, and H. Bériot. A comparison of high-order polynomial and wave-based methods for Helmholtz problems. *Journal of Computational Physics*, 321:105 – 125, 2016.
[24] J. Melenk and I. Babuška. The partition of unity finite element method: Basic theory and applications. *Computer Methods in Applied Mechanics and Engineering*, 139(1):289 – 314, 1996.
[25] J. M. Melenk and S. Sauter. Wavenumber explicit convergence analysis for Galerkin discretizations of the Helmholtz equation. *SIAM Journal on Numerical Analysis*, 49(3):1210–1243, 2011.
[26] S. W. Rienstra. Webster's horn equation revisited. *SIAM Journal on Applied Mathematics*, 65(6):1981–2004, 2005.
[27] T. Strouboulis, I. Babuška, and K. Copps. The design and analysis of the generalized finite element method. *Computer Methods in Applied Mechanics and Engineering*, 181(1-3):43 – 69, 2000.
[28] R. Tezaur, I. Kalashnikova, and C. Farhat. The discontinuous enrichment method for medium-frequency Helmholtz problems with a spatially variable wavenumber. *Computer Methods in Applied Mechanics and Engineering*, 268:126 – 140, 2014.
[29] J. Yuan, Y.-H. Pao, and W. Chen. Exact solutions for free vibrations of axially inhomogeneous Timoshenko beams with variable cross section. *Acta Mechanica*, 227(9):2625–2643, 2016.